Thermodynamic assessment of the neptunium-oxygen system: Mass spectrometrics studies and thermodynamic modelling

Smith, Anna; Colle, J-Y; Benes, O; Konings, Rudy; Sundman, B; Guéneau, C

Publication date
2016

Document Version
Final published version

Published in
The Journal of Chemical Thermodynamics

Citation (APA)
Smith, A., Colle, J.-Y., Benes, O., Konings, R., Sundman, B., & Guéneau, C. (2016). Thermodynamic assessment of the neptunium-oxygen system: Mass spectrometrics studies and thermodynamic modelling. *The Journal of Chemical Thermodynamics*, *103*, 257-275.

J. Chem. Thermodynamics 103 (2016) 257–275

Contents lists available at ScienceDirect

J. Chem. Thermodynamics

journal homepage: www.elsevier.com/locate/jct

Thermodynamic assessment of the neptunium–oxygen system: Mass spectrometric studies and thermodynamic modelling

A.L. Smith [a,b,c,*], J.-Y. Colle [b], O. Beneš [b], R.J.M. Konings [b], B. Sundman [d], C. Guéneau [e]

[a] Delft University of Technology, Radiation Science & Technology Department, Nuclear Energy and Radiation Applications (NERA), Mekelweg 15, 2629 JB Delft, The Netherlands
[b] European Commission, Joint Research Centre, P.O. Box 2340, D-76125 Karlsruhe, Germany
[c] Department of Materials Science and Metallurgy, University of Cambridge, 27 Charles Babbage Road, Cambridge CB3 0FS, United Kingdom
[d] Department of Materials Science and Engineering, Royal Institute of Technology, Stockholm, Sweden
[e] DEN/DANS/DPC/SCCME/LM2T – CEA Saclay, Bat.450 SE, 91191 Gif-sur-Yvette Cedex, France

ARTICLE INFO

Article history:
Received 2 May 2016
Received in revised form 20 July 2016
Accepted 24 July 2016
Available online 29 July 2016

Keywords:
CALPHAD
Knudsen effusion mass spectrometry
Neptunium–oxygen system

ABSTRACT

Knudsen effusion mass spectrometry measurements on neptunium dioxide are reported in this work, which have allowed to improve the understanding of its vapourization behaviour and solved discrepancies noticed in the literature: the enthalpy of formation of $NpO_2(g)$ has been re-assessed and the composition of neptunia at congruent vapourization has been determined at 2262 K. In addition, a thermodynamic model for the neptunium-oxygen system has been developed using the CALPHAD method. The non stoichiometric NpO_{2-x} phase is described herein using the compound energy formalism with ionic constituents $(Np^{3+}, Np^{4+})_1(O^{2-}, Va)_2$, while the liquid phase is represented with the ionic two-sublattice model $(Np^{4+})_P(O^{2-}, Va^{Q-}, O)_Q$. The reliability and consistency of all optimized Gibbs energies have been verified by calculating the phase equilibria, thermodynamic data, oxygen chemical potential and equilibrium partial pressures. Finally, a number of ill-defined data in the Np–O system have been identified after critical review of the literature and comparison with the present experimental results and CALPHAD model.

1. Introduction

A thorough knowledge of the inherent characteristics and behaviour under normal and accidental conditions of advanced nuclear fuels to which minor actinides have been incorporated, i.e., (U, Pu, Np, Am, Cm) O_2 fuel, is essential for the safe use of future Generation IV nuclear reactors. Temperatures can reach up to 2500 K in normal operating conditions at the centre of the fuel pin of Sodium-cooled Fast Reactors (SFRs), and about 773–1373 K on the pellet edge [1]. The prediction of the nature of the phases formed and their compositions under specific temperature and oxygen potential conditions is crucial from safety perspectives. Moreover, the determinations of the liquidus temperatures and vapourization processes are also needed in the scenario of an accident with uncontrolled temperature increase. In this context, the FUELBASE project has been initiated in 2005, which aims at providing a computational tool running thermodynamic calculations and assessing the behaviour of irradiated fuel materials (oxides, carbides, etc) containing fission products and minor actinides [2–4]. More recently, the international TAF-ID project has started in 2013 within the OECD/NEA, whose goal is to develop a thermodynamic database for nuclear materials in cooperation between several countries (www.oecd-nea.org/science/taf-id/).

The binary U–O, Pu–O and ternary U–Pu–O systems have been investigated extensively already, and thermodynamic models have been developed for these systems using the CALPHAD method [2,5,6]. The data available on the Np–O system are much more limited [7], however, and there is no satisfactory overall description using CALPHAD. Such a model has been reported by Kinoshita et al. in 2003, but it did not reproduce correctly all the available experimental data [7], and did not consider the vapourization behaviour. A thorough knowledge of this system is essential, however, and a sound description via models is needed for the heterogeneous in-pile recycling of Generation IV systems, where a high concentration of minor actinides is added to the UO_2 fuel assembly [8,9]. A CALPHAD model for the Np–O binary system has therefore been developed in this work using a ionic sublattice description

* Corresponding author at:Delft University of Technology, Radiation Science & Technology Department, Nuclear Energy and Radiation Applications (NERA), Mekelweg 15, 2629 JB Delft, The Netherlands.
E-mail address: a.l.smith@tudelft.nl (A.L. Smith).

http://dx.doi.org/10.1016/j.jct.2016.07.040
0021-9614/

compatible with already existing models of the FUELBASE and TAF-ID projects, with a particular emphasis on the replication of the vapour pressure equilibria in addition to the phase diagram, thermodynamic and oxygen potential data available in the literature. In addition, Knudsen effusion mass spectrometry (KEMS) measurements have been performed to complement the existing vapourization studies [10,11] and to solve discrepancies noticed in the literature.

A critical review of the phase diagram equilibria and thermodynamic functions available on the neptunium-oxygen system is firstly reported herein. The KEMS measurements are then described, which have allowed to re-evaluate the enthalpy of formation of NpO_2(g) and estimate the composition of neptunia at congruent vapourization at 2262 K. The sublattice models used for the CALPHAD modelling are furthermore presented. Finally, the calculated phase equilibria, thermodynamic, oxygen chemical potential, and vapourization data are assessed and compared with the experimental studies on this system.

2. Review of literature data on the Np–O system

2.1. Phase diagram data

Fig. 1 shows the Np–O phase diagram as reported by Richter and Sari [12], who performed ceramographic, X-ray diffraction, thermal, and electron microprobe analyses on stoichiometric and hypostoichiometric neptunium dioxide.

Neptunium metal exists in three allotropic forms: orthorhombic α-Np, tetragonal β-Np, and cubic γ-Np (Table 1), with transition

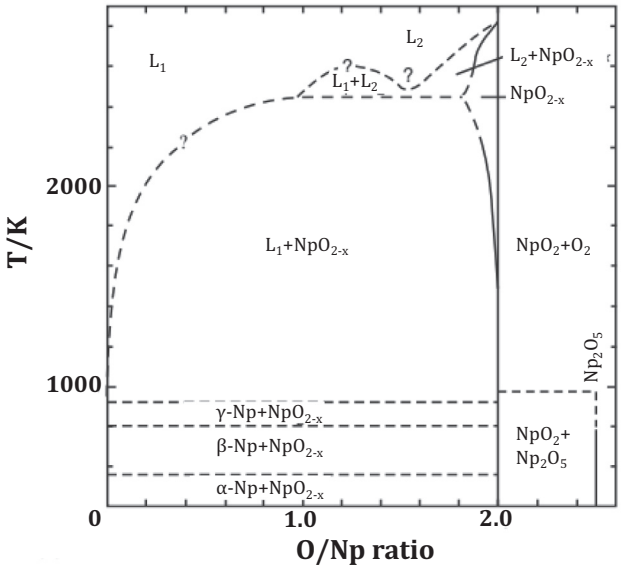

Fig. 1. Np–O phase diagram at 1 bar after Richter and Sari [12].

Table 1
Structural data for the Np–O system [17] (1 Å = 0.1 nm).

Phase	Symmetry	Space group	Lattice parameters/Å
α-Np	Orthorhombic	*Pnma*	a = 6.663 b = 4.723 c = 4.887 (at 293 K)
β-Np	Tetragonal	$P42_12$	a = 4.897 c = 3.388 (at 586 K)
γ-Np	Cubic	$Im\bar{3}m$	a = 3.518 (at 873 K)
NpO_2	Cubic	$Fm\bar{3}m$	a = 5.434
Np_2O_5	Monoclinic	P2/c	a = 4.188 b = 6.592 c = 4.090

temperatures and melting points at $T_{tr}(\alpha \rightarrow \beta) = (553 \pm 5)$ K, $T_{tr}(\beta \rightarrow \gamma) = (850 \pm 3)$ K, and $T_{fus}(\gamma) = (913 \pm 3)$ K, respectively [13]. The Np–O phase diagram shows an eutectic equilibrium $\{L_1 \rightarrow \gamma\text{-Np} + NpO_{2-x}\}$ at this same temperature $T_{eutectic} = (913 \pm 3)$ K [12]. The oxygen solubility limit in solid Np is not known, but assumed to be very low, by analogy with the U-O, Th-O, and Pu-O systems [7].

Two solid neptunium oxide phases have been identified, namely NpO_2(cr) and Np_2O_5(cr), with valence states (IV) and (V), respectively [7]. NpO_2 has a face-centred cubic crystal structure, in space group $Fm\bar{3}m$, while Np_2O_5 has monoclinic symmetry, in space group $P2/c$ (Table 1). The latter compound has been found highly unstable, with a decomposition to NpO_2(cr) and O_2(g) at about 700 K [7,12,14]. The existence of neptunium sesquioxide Np_2O_3 has been suggested in the vapour pressure studies of [10]. The X-ray (XPS) and Ultra-violet Photoelectron (UPS) spectroscopy studies of Naegele et al. [15] and Seibert et al. [16] have shown that the sesquioxide existed only as a transient species in the presence of neptunium metal, with a thickness of about 9 monolayers. The bulk species is not stable, and was therefore not considered in the present thermodynamic model.

The experimental studies of Richter and Sari have demonstrated the existence of a narrow hypostoichiometric homogeneity range for neptunium dioxide NpO_{2-x} above about 1300 K. Moreover, the recent high temperature X-ray diffraction measurements by Chollet et al. under air, He, and He/5%H_2 atmospheres have provided further proof for the reduction below the $NpO_{2.0}$ stoichiometry, with a departure from linearity of the lattice parameters towards higher values above 1643 K [18]. The departure from 1643 K to 1750 K has been attributed to the formation of oxygen vacancies only, while the formation of oxygen Frenkel pairs has also been suggested above the latter temperature [18]. The heat capacity and enthalpy increment data for NpO_2 cover the temperature range up to 1770 K [14,19]. There is no experimental evidence or quantification for the formation of oxygen Frenkel pairs in neptunium dioxide to this date: this would require to perform complementary measurements above 1770 K. But the latter behaviour is expected by analogy with the UO_2, PuO_2, and ThO_2 compounds, which show a steady increase in their heat capacity functions above about 2000 K because of this effect and its subsequent thermally induced disorder [20]. Konings and Beneš have recently estimated the contribution of oxygen Frenkel pairs formation on the high temperature heat capacity of NpO_2 by interpolation of the values for UO_2, PuO_2, and ThO_2 [20].

Regarding the melting point of neptunium dioxide, it has first been reported at (2833 ± 50) K by Chikalla et al. [21] and (2820 ± 60) K by Richter and Sari [12]. The recent measurement by Böhler et al. using a self-crucible laser heating technique has revealed a value about 250 K higher, however, i.e., (3070 ± 62) K [22,14]. The latter result is in better agreement with those for the isostructural UO_2, PuO_2, and ThO_2 compounds, and has therefore been selected in the present work. In addition, a possible hypostoichiometry of the congruently melting composition has been suggested [14].

A miscibility gap is expected in the liquid phase by analogy with the U–O, Th–O, and Pu–O systems, although there is no experimental evidence up to date. The oxygen solubility limit in liquid neptunium and the extent of this miscibility gap are also unknown [7]. Richter and Sari have suggested 2450 K for the monotectic equilibrium temperature, and an oxygen-to-metal ratio O/Np = 1.8 for the lower oxygen composition of the monophasic domain NpO_{2-x} at 2450 K, by extrapolation of the phase boundary curve from 2300 K.

Kinoshita et al. have published in 2003 a thermodynamic model for the Np–O system using the CALPHAD method [23], but the calculated diagram is not satisfying, with in particular the beginning of the hypostoichiometric homogeneity range of NpO_{2-x} at about

286 K, while Richter and Sari have reported it above 1300 K. In addition, the calculated phase boundary for the hypostoichiometric domain NpO_{2-x} does not follow the experimental points.

2.2. Thermodynamic data

2.2.1. Thermodynamic functions of pure elements and stoichiometric oxides

The thermodynamic functions of neptunium metal and stoichiometric oxides, NpO_2 and Np_2O_5, have recently been reviewed by Konings et al. [13,14]. The recommended data, which are listed in Tables 2 and 3, have been selected for the thermodynamic model.

2.2.2. Oxygen potential data

The only experimental study available on the variation of the oxygen potential of hypostoichiometric neptunium dioxide as a function of oxygen-to-metal ratio and temperature is by Bartscher and Sari [24]. The authors have used a gas-equilibrium method in the temperature range 1470 to 1850 K. Neptunium dioxide was heated on a thermobalance in a hydrogen-water atmosphere. The oxygen potential was subsequently derived from the known H_2O/H_2 ratio, and the corresponding O/Np ratio was calculated from the weight change of the sample. These oxygen potential lines, about midway between those of UO_{2-x} and PuO_{2-x} at a given temperature [7], are in good agreement with the trend of decreasing stability of the actinide dioxides along their series, i.e., from ThO_2 towards AmO_2.

In addition, Bartscher and Sari have estimated the phase boundary composition between NpO_{2-x} and $\{NpO_{2-x} + Np(l)\}$ in this same temperature range using their oxygen potential data combined with ceramographic and crystallographic analyses performed on quenched samples.

2.3. Vapourization studies

2.3.1. Thermodynamic functions of Np(g)

The enthalpy of formation of Np(g) has been assessed by Eick and Mulford [31] and Ackermann and Rauh [32] using the Knudsen effusion and mass spectrometry techniques. The neptunium metal sample used by the former set of authors showed about 0.56% plutonium impurity, however, and their results have therefore been discarded in the review by Konings et al. [13]. Konings et al. [13] have selected $\Delta_f H^o_m(Np, g, 298.15\ K) = (470 \pm 5)\ K$ after re-evaluation of the data of Ackermann and Rauh [32] collected on higher purity material (0.05% Pu). The entropy function, i.e., $S^o_m(Np, g, 298.15\ K) = (197.72 \pm 0.1)\ J \cdot K^{-1} \cdot mol^{-1}$, has been derived considering the electronic energy levels of a $^6L_{11/2}$ ground state and 670 excited states determined both experimentally and theoretically in the studies of [13,33–36].

Table 3
Summary of the heat capacity data for pure elements and stoichiometric oxides selected in the present work.

Phase	$C^o_{p,m}/(J \cdot K^{-1} \cdot mol^{-1}) = A + B \cdot (T/K) + C \cdot (T/K)^{-2}$			Ref.
	A	B	C	
α-Np(cr)	30.132	$-36.2372 \cdot 10^{-3}$	$1.1589 \cdot 10^{-4}$	[13]
β-Np(cr)	40			[13]
γ-Np(cr)	36			[13]
Np(l)	46			[13]
NpO_2(cr)	71.608	$15.845 \cdot 10^{-3}$	−900648	[19]
NpO_2(l)	66			[14]
Np_2O_5(cr)	99.2	$9.86 \cdot 10^{-2}$		[14,30]

2.3.2. Thermodynamic functions of NpO(g)

The enthalpy of formation of NpO(g) recommended in the review by Konings et al. [14] has been derived from the mass spectrometric measurements of Ackermann and Rauh on the two isomolecular reactions NpO(g) + La(g) = Np(g) + LaO(g) and Np(g) + YO(g) = NpO(g) + Y(g), respectively [37]. More details on this derivation are given in Section (5.4) and Appendix B. The value selected by [14] is $\Delta_f H^o_m(NpO, g, 298.15\ K) = -(16.6 \pm 10.0)\ kJ \cdot mol^{-1}$.

As there is no experimental data in the literature for the molecular constants and electronic structure of NpO(g), the standard entropy at 298.15 K and heat capacity function in the temperature range 298.15–4000 K have been derived in the work of [14] by analogy with similar systems. The electronic structure has been calculated based on the model of PmO(g), while the molecular constants have been estimated based on the trend shown by the lanthanide monoxides [14]. The derived function is $S^o_m(NpO, g, 298.15\ K) = (253.06 \pm 4.0)\ J \cdot K^{-1} \cdot mol^{-1}$.

2.3.3. Thermodynamic functions of NpO_2(g)

Vapour pressure studies of neptunium dioxide have been reported by Ackermann et al. [10] in 1966 and Gotcu-Freis et al. [11] in 2011 using the Knudsen effusion method. In the first case, the effusate was collected on platinum targets and subsequently analyzed by α-counting of ^{237}Np to derive the mass effusion rate and total pressure over the sample, assuming that one species was largely predominant in the gas phase (here NpO_2(g)). In addition, appearance potentials and relative changes in ionic intensities were measured with a time-of-flight mass spectrometer. In the second case, the gaseous vapour composition was directly analyzed using a quadrupole mass spectrometer, and the total and

Table 2
Summary of the thermodynamic data for pure elements and stoichiometric oxides selected in the present work.

Phase	$\Delta_f H^o_m(298.15\ K)/(kJ \cdot mol^{-1})$	$\Delta_{tr} H^o_m(T_{tr})/(kJ \cdot mol^{-1})$	$\Delta_{fus} H^o_m(T_{fus})/(kJ \cdot mol^{-1})$	$S^o_m(298.15\ K)/(J \cdot K^{-1} \cdot mol^{-1})$
α-Np(cr)	0	–	–	50.45 ± 0.40 [13,25]
β-Np(cr)	–	4.7 ± 0.5 [13,26]	–	–
γ-Np(cr)	–	3.0 ± 0.5 [13,26]	–	–
Np(l)	–	–	3.0 ± 0.5 [13,26]	–
NpO_2(cr)	−1078.5 ± 2.7 [14,27]	–	–	80.3 ± 0.4 [14,28]
NpO_2(l)	–	–	70.6 [14]	–
Np_2O_5(cr)	−2162.7 ± 9.3 [14,29]	–	–	186 ± 15 [14,29]

partial pressures were derived using silver as calibration standard material. Those studies have contributed to the understanding of the vapourization mechanism of neptunium dioxide on a number of points:

2.3.4. Vapourization mechanism

Those measurements have shown that neptunium dioxide becomes substoichiometric when heated at high temperatures under vacuum. Gotcu-Freis et al.reported the formation of $NpO_2(g)$ only when heating under oxygen flow up to 2200 K, with very little departure from stoichiometry [11]. But both sets of authors recorded the simultaneous formation of $NpO_2(g)$ and NpO(g) gaseous species when heating under vacuum in a tungsten cell, sign of the reduction of the condensed phase below stoichiometry [10,11]. Gotcu-Freis et al. even detected Np(g) under vacuum at 2500 K. These results show that Eqs. (2)–(4) should be considered next to the equilibrium reaction (1) for a correct assessment of the vapourization behaviour of neptunium dioxide:

$$NpO_2(cr) = NpO_2(g) \quad (1)$$

$$NpO_2(cr) = NpO_{2-x}(cr) + x/2O_2(g) \quad (2)$$

$$2NpO_{2-x}(cr) = NpO(g) + NpO_{2-x+y}(cr) + (1-x-y)/2O_2(g) \quad (3)$$

$$NpO(g) = Np(g) + 1/2O_2(g) \quad (4)$$

An important result from those studies was the relative small variation of the $NpO_2(g)$ partial pressure with respect to the sample's composition, by contrast with the NpO(g) partial pressure contribution, which was found to increase with the extent of substoichiometry.

2.3.5. Total and partial pressures over neptunium dioxide

Both sets of authors derived similar values for the total pressure over neptunium dioxide [11]. The curve of Ackermann et al. was obtained on a 300 mg sample. As less than 1% of the sample evaporated during their experiment, the authors assumed that $NpO_2(g)$ was the major species in the gas phase, and that the condensed phase referred to a quasi stoichiometric composition. The corresponding measurement was carried out with alternating temperature plateaus, i.e., with successively low and high temperatures, by contrast with the data of Gotcu-Freis et al., which were collected using a progressive ramp in temperature.

The measurement of Gotcu-Freis et al. was performed on less material (about 50–60 mg), and refers to a slightly more reduced composition. The authors reported a vapour made of 93% $NpO_2(g)$, 6% NpO(g), and 1% Np(g) at 2260 K under vacuum, with an overall gaseous composition $(O/Np)_{gas} = 1.939$ [11]. The authors assigned the same composition to their condensed phase, supposing a congruent equilibrium was reached in their experiment, but the latter interpretation must be adjusted. The vapour composition was directly analyzed after applying a 10 K/min heating ramp, with no stabilisation time at the investigated temperature (private communication), so as to stay as close as possible from a stoichiometric composition. This means their data refer to a slightly but continuously changing O/Np ratio. The composition of their condensed phase was therefore re-evaluated in the present work as detailed in Section 5.

2.3.6. Influence of the sample size

Ackermann et al. performed measurements on various sample sizes, which provides a valuable piece of information. The curve recorded by target collection on a 35 mg sample is shown in Fig. 4. In this case, a strong curvature was observed below 2100 K. The authors also noted that about 50% of the sample had evaporated after the three first data points (at successively 2129, 2304, and 1925 K) had been recorded. Such a behaviour can be related to the sample's thermal history, and especially to the alternating temperature plateaus used for the experiment which allow a rapid evolution of the sample's composition. The condensed phase was rapidly reduced below stoichiometry towards its congruent composition $(O/Np)_{cong,2304\,K}$ during the second temperature plateau at 2304 K. As the temperature was lowered to 1925 K for the third temperature plateau, the reduced composition $(O/Np)_{cong,2304\,K}$ was quenched to the new temperature. The latter composition is found below the stoichiometry at congruent vapourization at 1925 K, i.e., $(O/Np)_{cong,2304\,K} < (O/Np)_{cong,1925\,K}$, however. This subsequently generated a relative increase of total pressure, mainly due to NpO(g) and Np(g) species. The $NpO_2(g)$ contribution remained quasi unchanged during the process.

The smaller the sample is, the faster is the evolution at high temperatures, and therefore the more pronounced is this phenomenon, leading to more reduced compositions. This explains why a curvature was observed for the 35 mg sample, but not for the 300 mg sample. These experiments show that the thermal history of the neptunium dioxide material should be carefully considered when interpreting the results.

2.3.7. Sublimation enthalpy of NpO_2(cr)

The enthalpy of sublimation of neptunium dioxide has been derived from those vapour pressure measurements by second and third law analyses. Ideally, the measurement should refer to perfectly stoichiometric $NpO_{2.0}$, and to the equilibrium reaction (1) for an accurate and sound determination of the enthalpy of sublimation. This can only be achieved under oxygen flow, and Gotcu-Freis et al. found $\Delta_{sub}H^o_m(298.15\ K) = 650\ kJ \cdot mol^{-1}$ by second law treatment of their data [13]. The authors could unfortunately not perform a third law analysis because the pressure calibration failed (private communication).

Konings et al. prefer in their review to select the data of Ackermann et al. acquired under vacuum on the 300 mg sample with quasi-stoichiometric composition [10,14]. The enthalpies of sublimation determined by second and third law methods are in very good agreement: $\Delta_{sub}H^o_m(298.15\ K) = (623.2 \pm 12)\ kJ \cdot mol^{-1}$ and $\Delta_{sub}H^o_m(298.15\ K) = (619.5 \pm 10)\ kJ \cdot mol^{-1}$, respectively. The mean value has been selected in the review: $\Delta_{sub}H^o_m(298.15\ K) = (621 \pm 20)\ kJ \cdot mol^{-1}$ [14], which corresponds to an enthalpy of formation of $NpO_2(g)$ at 298.15 K as $\Delta_f H^o_m(NpO_2, g, 298.15\ K) = -(457 \pm 20)\ kJ \cdot mol^{-1}$ [14] when combined with the enthalpy of formation of NpO_2(cr) [14].

The standard entropy and heat capacity functions used in this work for $NpO_2(g)$ are those recommended by [14]. The molecular structure and spectra of $NpO_2(g)$ have never been investigated experimentally. The ground state was assumed to be $^4H_{3.5\ g}$ based on the DFT calculations of Infante et al. at the SO-CASPT2 level [38], and the associated vibrational frequencies were taken from the calculations of [39]. As for the electronic energy levels, they were calculated based on the crystal field model of monoclinic neptunium tetrafluoride which shows a C_2 site symmetry [14]. The derived entropy value is $S^o_m(NpO_2, g, 298.15\ K) = (269.892 \pm 6.0)\ J \cdot K^{-1} \cdot mol^{-1}$.

3. Mass spectrometric investigations

In the present work, KEMS measurements were carried out on the same device as the one used by Gotcu-Freis et al. [11], both under oxygen flow and under vacuum. As detailed in the previous section, the measurements of Ackermann et al. carried out with alternating temperature plateaus refer to slightly changing compositions below stoichiometry. Measurements under oxygen flow were therefore performed so as to re-evaluate the sublimation enthalpy of NpO_2(cr), and thereafter standard enthalpy of formation of $NpO_2(g)$, while maintaining the composition of the

sample as close as possible from the stoichiometric O/Np = 2 phase boundary. The studies under vacuum were performed in an attempt to reach the congruent state composition. By contrast with the work of Gotcu-Freis et al. [11], the composition of the vapour formed above neptunia was investigated after several hours of heating at constant temperature and not directly after the heating ramp. Care was taken to wait for constant signals, sign of the attainment of a steady state. The influence of the heating time on the extent of substoichiometry was hence assessed by comparison with the results of Gotcu-Freis et al., and the corresponding O/Np ratios of the gaseous and condensed phases were derived. In addition, the obtained partial pressures were compared with the ones calculated with our thermodynamic model at congruent vapourization.

3.1. Material and method

The neptunium dioxide material ($^{237}NpO_2$ from ORNL, Oak Ridge National Laboratory, mass fraction purity > 0.998) (Table 4) was first heated under O_2 flow at 923 K for 12 h in a tubular furnace because of the slight hypostoichiometric homogeneity range reported by Richter and Sari [12]. The X-ray pattern revealed a cubic fluorite structure with cell parameter 5.4340(5) Å. This is in very good agreement with the value reported in the literature (5.4338 Å) [17], indicating that the starting neptunium dioxide was pure and stoichiometric.

The X-ray diffraction (XRD) measurements were performed at (295 ± 2[1]) K using a Bruker D8 X-ray diffractometer mounted in the Bragg–Brentano configuration, with a curved Ge monochromator (111), a ceramic copper tube (40 kV, 40 mA), and equipped with a LinxEye position sensitive detector. The data were collected by step scanning in the angle range $10^\circ \leqslant 2\theta \leqslant 120^\circ$, with an integration time of about 8 h, a count step of $0.02^\circ(2\theta)$, and a dwell of 5 s/step. Structural analysis was performed by the Rietveld method with the Fullprof2k suite [40].

The experimental set up used in the present work consisted of a Knudsen effusion cell coupled to a quadrupole mass spectrometer (QMG422, Pfeiffer Vacuum GmbH). The sample of interest was placed in the Knudsen cell (made either of tungsten or {ZrO_2+Ir liner}), and heated under vacuum or in the presence of a controlled oxygen pressure, in a high temperature furnace made of tungsten-coil heating elements, and surrounded by seven cylindrical thermal shields (three in tungsten, four in tantalum). The choice of the tungsten and {ZrO_2+Ir} materials for the Knudsen cell was based on their high melting points, and low reactivity with respect to actinide materials [41]. The furnace itself was placed in a high vacuum chamber (10^{-7}–10^{-8} mbar). The vapour species effusing through the orifice at the top of the cell were subsequently ionized with a cross beam electron bombardment ion source. The dimensions of the orifice of the Knudsen cell were specifically chosen to ensure that the effusing beam remained in a molecular flow regime [42]. The quadrupole mass spectrometer, equipped with an axial Faraday cup, and a 90°Second Electron Multiplier (SEM) detector connected to an electrometer, was used for the ion current measurement and analysis of the mass spectrum of the beam effusing through the orifice of the cell. The mass spectrometer covered the range of 1 to 512 atomic mass unit (amu). The temperature was monitored using an optical pyrometer. It was calibrated by measuring the melting points of standard materials (Ag, Zn, Cu, Fe, Pt, Al_2O_3), identified as small plateaus on the vapour pressure curve. Its associated uncertainty is estimated to be ±10 K. The whole apparatus, specifically designed to study radioactive materials, was finally placed in a glove box shielded by a 5 cm thick lead. A schematic drawing of the setup was given in another publication [43].

Table 4
Provenance and purity of the neptunium dioxide material used in this study.

Formula	Source	State	Analysis	Mass fraction purity
NpO_2	ORNL	Powder	XRD	>0.998

The vapourization behaviour of neptunium dioxide was studied in both reducing (under vacuum using 65.35 mg of material) and oxidizing conditions (under oxygen flow using 14.94 mg of material). The first set of measurements was carried out in a tungsten cell, while the second set was performed in a ZrO_2 cell with an additional iridium liner placed at the bottom to avoid possible chemical interactions at high temperatures between sample and containment material (Fig. 2). The ZrO_2 cell assembly shown in Fig. 2 moreover had a small orifice at the bottom for the oxygen gas inlet (diameter $d < 0.5$ mm). The oxygen gas introduced into the cell was of high-grade purity (mass fraction purity 0.99999). The flow was moreover controlled and monitored during the whole experiment. The temperature was increased gradually at a heating rate of 10 K/min, and the species vaporizing from the neptunium dioxide sample analyzed with the mass spectrometer at 30 eV ionization electron energy. At the end of the measurement, the temperature was rapidly decreased, and the sample analyzed by X-ray diffraction. The corresponding X-ray diffraction patterns showed in both cases single phase neptunium dioxide materials with cell parameters as 5.4341(5) Å and 5.4334(5) Å for the measurements under vacuum and oxygen flow, respectively. No secondary phases indicative of possible interactions between the sample and cell material were detected.

Under the electron beam bombardment, the vapour species i can undergo either direct ionization, or fragmentation to a number of ions k, j, n, etc. The vapour pressure of species i in the gas phase, P_i, is related to the intensity of the molecular beam recorded for the ion k formed from species i, I^+_{ik}, to the actual temperature, T, and to a sensitivity factor specific to ion k, S_{ik}, as expressed in Eq. (5) [42]:

$$P_i = I^+_{ik} \cdot T / S_{ik} \tag{5}$$

The sensitivity factor, S_{ik}, is furthermore related to an instrumental factor, K_g, independent of the ion detected, to the ion partial ionization cross-section, σ_{ik}, isotopic abundance, f_{ik}, and to the efficiency of the second electron multiplier, γ_{ik}, according to:

$$S_{ik} = K_g \cdot \sigma_{ik} \cdot \gamma_{ik} \cdot f_{ik} \tag{6}$$

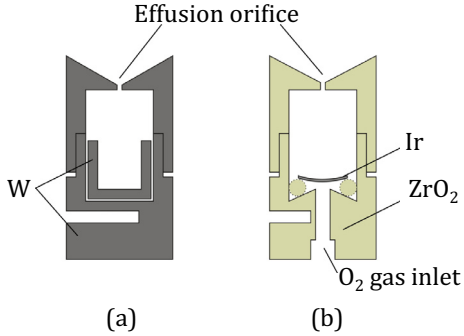

Fig. 2. The Knudsen cell assembly made of (a) tungsten and (b) ZrO_2+Ir liner used for the KEMS measurements under vacuum and oxygen flow, respectively.

[1] The quoted uncertainty corresponds to the standard uncertainty.

All isotopic contributions are added before treatment of the data, meaning f_{ik} equals unity. The instrumental factor, K_g, is estimated by vaporizing a known quantity of silver together with the sample. Silver vaporizes in the temperature range 1200–1500 K, has a well-known vapour pressure [44], and stays relatively inert in the system, which makes it an ideal reference material for calibration. For atomic species, the partial and total ionization cross sections are identical. When molecular species are involved, parent ions are formed by direct ionization, while fragment ions might also appear due to dissociation (fragmentation) processes.

The partial pressure of species i can be expressed as a function of the total ionization cross section and intensities of the parent and fragment ions as follows:

$$P_i = \frac{1}{K_g \cdot \overline{\sigma_i}} \cdot \left(\frac{I^+_{par\,k} \cdot T}{\gamma_{ik}} + \frac{I^+_{frag\,j} \cdot T}{\gamma_{ij}} + \cdots + \frac{I^+_{frag\,n} \cdot T}{\gamma_{in}} \right) \quad (7)$$

We refer the reader to [45] for further detail on the derivation of this equation. In the latter relation, the efficiency of the second electron multiplier can be approximated as $\gamma_{ik} = \delta/M_{ik}^{1/2}$, where M_{ik} is the molar mass of ion k, and δ is a constant, following Grimley [46].

The atomic ionization cross-sections of neptunium and oxygen were estimated using the program SIGMA [42,47,48] and data of Mann [47]. The total ionization cross sections of NpO(g) and NpO_2(g) gaseous species were calculated using the modified additivity rule, as described by Deutsch et al. [49,50] ($\sigma(NpO) = 12.9 \cdot 10^{-16}$ cm^2, $\sigma(NpO_2) = 11.2 \cdot 10^{-16}$ cm^2 at 30 eV). The ionization cross sections of WO(g), WO_2(g), and WO_3(g) were taken from the calculations of Deutsch et al. using the DM formalism [51] ($\sigma(WO) = 6.6 \cdot 10^{-16}$ cm^2, $\sigma(WO_2) = 4.5 \cdot 10^{-16}$ cm^2, $\sigma(WO_3) = 3.5 \cdot 10^{-16}$ cm^2 at 30 eV).

Ionization efficiency curves were recorded at specific temperatures along the KEMS measurement to get a better insight into the ionization and dissociation (fragmentation) mechanisms of the species monitored, and therefore chemical composition of the gas. Isothermal scans of the ion intensities were obtained by increasing the cathodic voltage stepwise by 0.5 eV. A calibration curve was used to correct for the offset between the applied cathodic voltage and the effective electron energy, covering the energy range 10.3 to 22 eV, based on the first ionization potentials of silver (7.576 eV), zinc (9.393 eV), indium (5.786 eV), and a known gas composition of argon (15.759 eV), xenon (12.129 eV), and krypton (13.999 eV) [42]. The measured offset showed a satisfying linear dependence (with a regression factor of 0.975), which was extrapolated up to 40 eV applied cathodic voltage.

A more detailed description of the derivation of the total and partial pressures of the various species detected, as well as of the procedure applied to correct the signals for fragmentation, was given in other publications [45,52].

3.2. Measurements under vacuum

Neptunium dioxide was heated up to 2260 K, and maintained at this temperature for several hours (about 3 h), until all signals recorded had reached constant levels. Ionization efficiency curves, shown in Fig. 3, were subsequently recorded to provide insight into the vapour composition. The appearance potential data recorded are listed in Table 5, together with the associated ionization and dissociation processes, and a comparison with literature data.

NpO(g) and NpO_2(g) were both present in the vapour, but no Np (g) was observed. Furthermore, it is worth pointing out that O(g) and O_2(g) were not detected, mainly due to the high background level at those low masses. At 12 eV, i.e., just before the dissociation energy of NpO_2 into NpO^+, the signal of NpO_2^+ was about 1.5 times that of NpO^+. In the measurement of Gotcu-Freis et al., this ratio

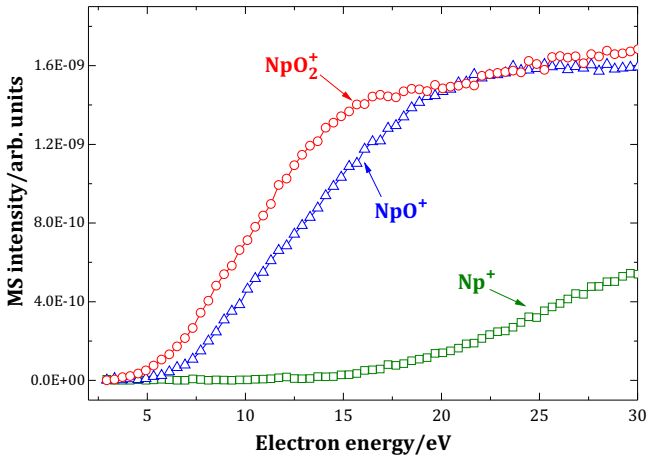

Fig. 3. Ionization efficiency curves of Np^+ (□), NpO^+ (△), and NpO_2^+ (○) recorded at T = 2262 K after 3 h of stabilisation time at about 2260 K.

Table 5
Ionization and appearance potentials recorded at 2262 K. In the work of Gotcu-Freis et al. [11], the ionization energies were measured at 2500 K on a reduced NpO_2 sample following high temperature treatment. The dissociation energies were measured at 2200 K under oxidative conditions.

Process	Potential/eV (this work)	Potential/eV [11]
$NpO_2 + e^- \rightarrow NpO_2^+ + 2e^-$	6.2 ± 0.4	5.6 ± 0.3
$NpO_2 + e^- \rightarrow NpO^+ + O + 2e^-$	12.0 ± 1.2	12.5 ± 0.6
$NpO_2 + e^- \rightarrow Np^+ + 2O + 2e^-$	20.7 ± 0.7	20.5 ± 1
$NpO + e^- \rightarrow NpO^+ + 2e^-$	7.0 ± 0.4	6.0 ± 0.3
$NpO + e^- \rightarrow Np^+ + O + 2e^-$	13.8 ± 0.6	13.0 ± 0.6

was more than 4 at 2260 K [11]. This difference can be related to a longer heating time of our sample at the investigated temperature, and therefore greater reduction, as expected from the vapourization mechanism detailed in Eqs. (1)–(4).

The partial pressures P_{Np}, P_{NpO}, and P_{NpO_2} were subsequently obtained after correction for the dissociation processes, yielding for the vapour composition at 2262 K: 85.2% NpO_2(g) and 14.8% NpO(g). This is more reduced than in the work of Gotcu-Freis et al. (93% NpO_2(g), 6% NpO(g) and 1% Np(g) at 2260 K) as a consequence of the longer heating time. Ackermann et al. also performed ionization potential measurements on a "well-aged sample" at slightly higher temperature, i.e., 2300 K. The authors found about 2/3 of NpO_2(g) and 1/3 of NpO(g) in the gas phase, but these figures should be considered with care as the authors did not report the thermal history of their sample. The latter was probably heated several hours before being analyzed, but it is not clear at which temperature. The reported composition could hence correspond to congruent vapourization, but also to a more reduced stoichiometry if the sample was heated previously at a higher temperature than 2300 K.

The composition of the gaseous phase was subsequently assessed from the ratio of the atomic flows between oxygen and neptunium, F_O/F_{Np} [53]. F_O and F_{Np} are expressed as a function of temperature, partial pressure, and molar mass of the species vaporizing using the appropriate Hertz–Knudsen relations (8) [53–55] according to:

$$F_O = sC/(2\pi RT)^{1/2} \cdot \left[P_O/(M_O)^{1/2} + P_{NpO}/(M_{NpO})^{1/2} + 2P_{NpO_2}/(M_{NpO_2})^{1/2} + 2P_{O_2}/(M_{O_2})^{1/2} \right]$$

$$F_{Np} = sC/(2\pi RT)^{1/2} \cdot \left[P_{Np}/(M_{Np})^{1/2} + P_{NpO}/(M_{NpO})^{1/2} + P_{NpO_2}/(M_{NpO_2})^{1/2} \right] \quad (8)$$

where s is the area of the effusion orifice, C the Clausing factor, M_i the molar mass, P_i the partial pressure, T the temperature, and R the universal gas constant.

Considering only the NpO and NpO_2 partial pressures measured experimentally (P_{Np} being negligible in the present case) and their molar masses for the given temperature, the calculation leads to an oxygen-to-metal ratio in the gas equal to $F_O/F_{Np} = (1.849 \pm 0.003^{1})$ at 2262 K. When performing the same calculation, Gotcu-Freis et al. obtained $F_O/F_{Np} = (1.939 \pm 0.003^{1})$ at 2260 K. P_O and P_{O_2} partial pressures cannot be measured experimentally because of the high background level at low masses. However, they can be estimated from the following equilibrium reactions (9) and (10) and their associated theoretical equilibrium constants as described by Beneš et al. [52]:

$$NpO(g) + \frac{1}{2}O_2(g) = NpO_2(g) \tag{9}$$

$$NpO(g) + O(g) = NpO_2(g) \tag{10}$$

The Gibbs energy of reaction and theoretical equilibrium constant, K_P, associated with reaction (9) are given by Eqs. (11) and (12):

$$\begin{aligned}\Delta_r G^{o}_{m}(T/\mathrm{K}) &= -R(T/\mathrm{K})\ln K_P \\ &= \Delta_f G^{o}_{m}(NpO_2, g, T/\mathrm{K}) - \Delta_f G^{o}_{m}(NpO, g, T/\mathrm{K}) \\ &\quad - 0.5\Delta_f G^{o}_{m}(O_2, g, T/\mathrm{K})\end{aligned} \tag{11}$$

$$K_P = \frac{P_{NpO_2}}{P_{NpO} \cdot (P_{O_2})^{1/2}} \tag{12}$$

where $\Delta_f G^{o}_{m}(\mathrm{NpO_2, g}, T/\mathrm{K})$, $\Delta_f G^{o}_{m}(\mathrm{NpO, g}, T/\mathrm{K})$ and $\Delta_f G^{o}_{m}(\mathrm{O_2, g}, T/\mathrm{K})$ are the standard Gibbs energies of formation of the gaseous species NpO_2(g), NpO(g) and O_2(g), respectively, and P_{NpO_2}, P_{NpO} and P_{O_2} their partial pressures.

Using those equations, the equilibrium partial pressure of oxygen P_{O_2} can be estimated from the experimentally determined vapour pressures of Np bearing species. A similar procedure applied to Eq. (10) allows to derive P_O. Considering all four partial pressures, i.e., P_{NpO} and P_{NpO_2} (determined experimentally), P_O (calculated) and P_{O_2} (calculated), the oxygen-to-metal ratios in the gas phases are derived as $\boldsymbol{F_O/F^{*}_{Np}} = (\mathbf{1.856 \pm 0.003}^{1})$ and $\boldsymbol{F_O/F^{*}_{Np}} = (\mathbf{1.967 \pm 0.003}^{1})$ based on the present data and that of Gotcu-Freis et al., respectively.

After several hours of heating at constant temperature and subsequent ionization efficiency measurement, the sample was cooled down by 110 K, and heated up again with a ramp of 10 K/min from 2150 to 2260 K. The total and partial vapour pressures corrected for the dissociation processes are shown in Fig. 4, together with the total pressures recorded by Ackermann et al. and Gotcu-Freis et al. The total pressure collected herein is similar to that measured in the previous studies. The contribution from NpO(g) is higher, however, due to the greater reduction. A similar behaviour was observed for hypostoichiometric uranium dioxide, with a rather constant UO_2(g) partial pressure, but increased UO(g) contribution as the uranium dioxide becomes more reduced [7].

The total pressure of neptunium bearing species and NpO_2(g) partial pressure, obtained after several hours of stabilisation, can be represented by the following least-squares equations[2] in the temperature range 2150–2260 K:

$$\ln(P_{tot}/\mathrm{Pa}) = 28.98(\pm 0.07) - 66,521(\pm 156) \cdot (T/\mathrm{K})^{-1} \tag{13}$$

$$\ln(P_{NpO2}/\mathrm{Pa}) = 28.87(\pm 0.07) - 66,687(\pm 163) \cdot (T/\mathrm{K})^{-1} \tag{14}$$

[2] The quoted uncertainties correspond to the standard deviation on the least-squares fitting.

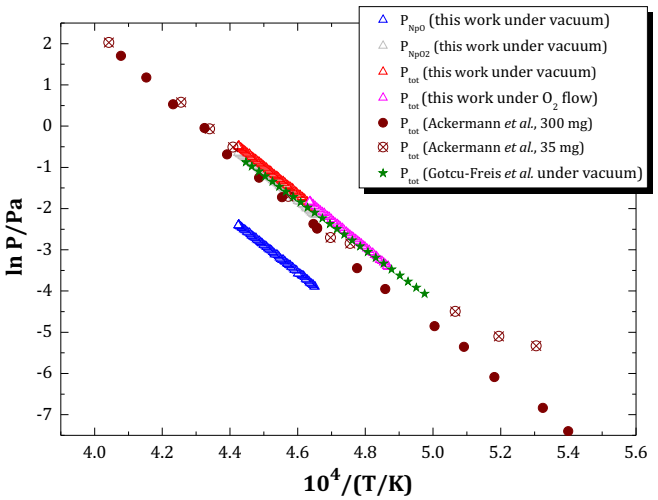

Fig. 4. Total pressure of neptunium bearing species (△), NpO_2(g) (△), and NpO(g) (△) partial pressures recorded in the present work under vacuum after several hours of stabilisation, and corresponding to a vapour composition $(O/Np)_{gas} = 1.856$ (3) at 2262 K (see text). Total pressure of neptunium bearing species collected under oxygen flow (△). Literature data of Ackermann et al. for the total pressure over a 300 mg sample with quasi-stoichiometric composition (●), and over a 35 mg sample (⊗) [10]. Total pressure recorded by Gotcu-Freis et al. directly after the temperature ramp, and corresponding to a vapour composition $(O/Np)_{gas} = 1.967(3)$ (see text) (⋆) [11].

Using the second law of thermodynamics applied to the NpO_2(g) signal only and the auxiliary data recommended in Section 2.2.1, the enthalpy of sublimation was estimated as $\Delta_{sub}H^{o}_{m}(298.15\ \mathrm{K}) = (603.7 \pm 2.0^{1})\ \mathrm{kJ \cdot mol^{-1}}$. The third law analysis yielded $\Delta_{sub}H^{o}_{m}(298.15\ \mathrm{K}) = (610.4 \pm 0.2)\ \mathrm{kJ \cdot mol^{-1}}$, in reasonable agreement with the second law value. The uncertainty assigned to the latter result corresponds to the standard deviation only, not accounting for the uncertainties on pressure calibration, corrections for the fragmentation pattern, and the uncertainties in the thermal functions.

The derived enthalpies should be considered with care, however, as the stoichiometry of the measured sample was relatively far from $NpO_{2.0}$. Since the NpO_2(g) partial pressure is relatively insensitive to the O/Np ratio, as reported in the literature, the derived sublimation enthalpy of NpO_2(cr) should not be affected too much by the extent of substoichiometry. But a measurement under O_2 flow is needed to derive a more accurate value for the sublimation enthalpy of neptunium dioxide as described in the next section.

3.3. Measurements under oxygen flow

The temperature profile used for the measurements under oxygen flow is shown in Fig. 5. Appearance potential (AP) curves, indicated as AP_i ($i = 1 \ldots 6$) in Fig. 5, were recorded at several points during the experiment to provide insight into the vapour composition. Using those data, the real partial pressures P_{Np}, P_{NpO}, and P_{NpO_2} were corrected as described previously for the dissociation processes along the measurement. The composition of the vapour at the various points is listed in Table 6.

The analysis of the ionization efficiency curves revealed only NpO_2(g) gaseous species at 2060 K (AP_1) under the applied oxygen pressure. Neither NpO(g) nor Np(g) were detected. However, NpO (g) was found in the vapour after the first ramp in temperature up to 2256 K ($Ramp_A$) at a level of about 5.3% (AP_2). The oxygen pressure applied in the cell was thereafter slightly increased in the second part of the experiment (AP_4 to AP_6) to be above the

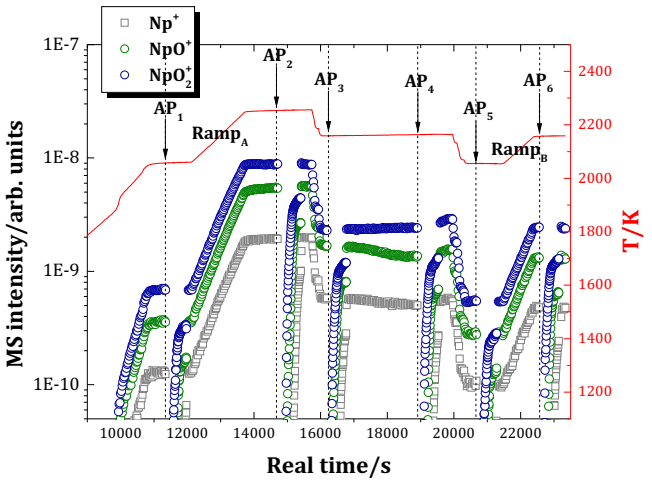

Fig. 5. Evolution of the temperature profile and mass spectrometric intensities of Np^+, NpO^+, and NpO_2^+ during the Knudsen effusion mass spectrometry measurement under oxygen flow.

equilibrium pressure for NpO_2(cr), while taking care that we remained in Knudsen conditions.

As it was not possible to determine the oxygen pressure in the Knudsen cell by direct measurement of the mass spectrometer, we have assessed the value of the imposed oxygen pressure based on the Hertz-Knudsen relation:

$$\frac{dN_i}{dt} = \frac{P_i s C}{\sqrt{2\pi M_i RT}} \tag{15}$$

in which P_i is the pressure of oxygen to be determined, M_i is the molar mass of the molecule, R is the gas constant, T the absolute temperature, s the surface of the orifice through which the gaseous molecules escape from the cell, and C the Clausing factor which accounts for the shape of the effusion orifice, and its non negligible depth [56]. The flow of the molecules (dN_i/dt) is expressed in mol/s and is determined based on the knowledge of the pump speed used to pump the gaseous products from the vacuum vessel, and the pressure of oxygen measured by the pressure gauge within the vessel. The former parameter was assessed based on the pump characteristics and exact measurement of its frequency of rotations, while the pressure of oxygen in the vessel was obtained as difference in the total pressure measured with oxygen flow and without. With the thus determined two parameters, the flow of oxygen is calculated using the ideal gas equation. Coupling the mass flow with the Hertz-Knudsen equation, the calculated oxygen pressure in the cell ranged from 8.9 Pa at 2056 K (AP_5) to 9.1 Pa at 2159 K (AP_6), thus lower than the limit of the Knudsen conditions which is for our geometrical set-up at 11.3 Pa.

The higher oxygen potential allowed to re-oxidize the neptunium dioxide sample: the analysis at 2164 K (AP_4) showed only 1.2% NpO(g). The total and partial vapour pressures subsequently recorded on the second temperature ramp ($Ramp_B$) between 2056 K (AP_5 with 100% NpO_2(g)) and 2159 K (AP_6 with 98.8% NpO_2(g) and 1.2% NpO(g)) correspond to a quasi-stoichiometric neptunium dioxide sample, with a composition very close to the stoichiometric O/Np = 2 phase boundary. These data can therefore be used to derive the sublimation enthalpy of NpO_2(cr) with a higher degree of confidence with respect to the oxygen-to-metal ratio compared to previous measurements.

The total pressure of neptunium bearing species and NpO_2(g) partial pressure corrected for the small contribution of NpO(g) (1.2% according to the analysis AP_6) can be represented by the following least-squares equations[2] in the temperature range 2060–2150 K:

$$\ln(P_{tot}/\text{Pa}) = 29.48(\pm 0.10) - 67,536(\pm 214)\cdot(T/\text{K})^{-1} \tag{16}$$

$$\ln(P_{NpO2}/\text{Pa}) = 29.46(\pm 0.10) - 67,525(\pm 213)\cdot(T/\text{K})^{-1} \tag{17}$$

Using the second law of thermodynamics applied to the NpO_2(g) signal only and the auxiliary data recommended in Section 2.2.1, the enthalpy of sublimation was estimated with Eq. (1) as $\Delta_{sub}H^o_m(298.15\ \text{K}) = (606.9 \pm 1.9^{1})\ \text{kJ·mol}^{-1}$. The third law analysis yielded $\Delta_{sub}H^o_m(298.15\ \text{K}) = (606.7 \pm 0.2)\ \text{kJ}\cdot\text{mol}^{-1}$, in very good agreement with the second law value. The good accordance results from the careful control of the O/Np stoichiometry during the temperature ramp. It is also worth pointing out that the latter data are very close to those derived under vacuum (see Section 3.2). The sublimation enthalpy of NpO_2(cr) finally retained and recommended in this work is taken as the average value of the second and third law treatments under oxygen flow, i.e., $\mathbf{\Delta_{sub}H^o_m(298.15\ K) = (606.8 \pm 1.9^{1})\ kJ\cdot mol^{-1}}$. Using the standard enthalpy of formation of NpO_2(cr) recommended by [14], the standard enthalpy of formation of NpO_2(g) is finally derived as $\mathbf{\Delta_f H^o_m(NpO_2, g, 298.15\ K) = -(471.7 \pm 3.3^{1})\ kJ\cdot mol^{-1}}$.

4. Thermodynamic modelling

The PARROT module of the Thermo-Calc software (Version 2015b) was used to optimize the thermodynamic parameters of all phases in the neptunium-oxygen system [57,58]. The oxygen solubility in the different allotropic forms of neptunium was neglected in this work. Np_2O_5 was treated as a stoichiometric compound. The Gibbs energy functions of all the phases are referred to the enthalpy of the pure elements in their stable state at room temperature 298.15 K and 1 bar ($^oH_i^{SER}$(298.15 K)).

4.1. Pure elements

The Gibbs energy functions of the pure elements i at temperature T and in their state φ are given by:

$$G_i^{\varphi}(T) - {}^oH_i^{SER}(298.15\ \text{K}) = a + b\cdot T + c\cdot T\cdot\ln T + \sum d_n T^n \tag{18}$$

Table 6
Vapour pressure composition along the experiment under oxygen flow, and atomic flow ratio in the gas phase. F_O/F_{Np} was calculated considering only P_{NpO} and P_{NpO2} measured experimentally. F_O/F^*_{Np} was calculated taking the equilibrium P_O and P_{O2} partial pressures into account (estimated using Eqs. (9) and (10)).

	T[a]/K	Vapour composition/(%)		F_O/F_{Np}[b]	F_O/F^*_{Np}[b]
		NpO(g)	NpO_2(g)		
AP_1	2060	0	100	2.000	–
AP_2	2256	5.3	94.7	1.945	1.966
AP_3	2160	11.1	88.9	1.886	1.892
AP_4	2164	1.2	98.8	1.988	2.054
AP_5	2056	0	100	2.000	–
AP_6	2159	1.2	98.8	1.987	2.068

[a] Standard uncertainties u are $u(T) = 10$ K.
[b] Standard uncertainties u are $u(F_O/F_{Np}) = 0.003$.

where n is an integer (2, 3, −1…). In the present work, the parameters reported by Dinsdale were used for pure neptunium and oxygen [59].

4.2. Stoichiometric neptunium oxide Np_2O_5

The Np_2O_5 oxide was described with the $(Np^{5+})_2(O^{-2})_5$ two-sublattice model. The corresponding Gibbs energy function has the same form as in Eq. (18):

$$G^{\varphi}(T) - \sum n_i^{\varphi o} H_i^{SER}(298.15\ \mathrm{K}) = a + b\cdot T + c\cdot T\cdot \ln T + \sum d_n T^n \tag{19}$$

where n_i^{φ} is the number of atoms of the ith element in the oxide formula. The Gibbs energy function of Belyaev et al. [30], recommended in the review of [14], was taken to initialize the parameters. The coefficients a and b were subsequently optimized.

4.3. NpO_{2-x} phase

NpO_2, like UO_2, ThO_2, and PuO_2, adopts a fluorite type lattice with a marked ionic character. NpO_{2-x} was hence described herein using the compound energy formalism with ionic species, as was done for $UO_{2\pm x}$ [2,5] and PuO_{2-x} [2,6]:

$$(Np^{3+}, Np^{4+})_1(O^{2-}, Va)_2 \tag{20}$$

The first sublattice is the site for cations, and the second sublattice the normal site for oxygen in the fluorite structure where the addition of vacancies allows the description of the hypostoichiometric region NpO_{2-x}. A more general notation is $(Np^{3+}, Np^{4+})_1(O^{2-}, Va)_2(O^{2-}, Va)_1$, the third sublattice being the site for interstitial oxygen, which represents the hyperstoichiometric composition range NpO_{2+x}. But the latter sublattice is not required to describe the Np–O system as neptunium dioxide cannot be oxidized above $NpO_{2.0}$ [12]. It would be needed to assess mixed oxide systems such as $(U,Np)O_{2\pm x}$, however. Because the phase has to remain electronically neutral at equilibrium, the addition of Np^{3+} species on the first sublattice is necessary to compensate the presence of oxygen vacancies on the normal site for oxygen in the second sublattice.

The Gibbs energy of the hypostoichiometric oxide phase is expressed as:

$$\begin{aligned} G^{\varphi} - \Sigma n_i^{\varphi o} H_i^{SER}(298.15\ \mathrm{K}) = {} & y_{Np^{4+}} y_{O^{2-}} \cdot {}^{o}G_{(Np^{4+})_1(O^{2-})_2} + y_{Np^{4+}} y_{Va} \cdot {}^{o}G_{(Np^{4+})_1(Va)_2} \\ & + y_{Np^{3+}} y_{O^{2-}} \cdot {}^{o}G_{(Np^{3+})_1(O^{2-})_2} + y_{Np^{3+}} y_{Va} \cdot {}^{o}G_{(Np^{3+})_1(Va)_2} \\ & + RT(y_{Np^{4+}} \ln y_{Np^{4+}} + y_{Np^{3+}} \ln y_{Np^{3+}}) \\ & + 2RT(y_{O^{2-}} \ln y_{O^{2-}} + y_{Va} \ln y_{Va}) \end{aligned} \tag{21}$$

where y_i are the fractions of species i in the sublattice, and ${}^{o}G_{(i)_1(j)_{(2)}}$ are the Gibbs energies of the different compounds formed by considering the species i on the first sublattice and j on the second sublattice. The Gibbs energy of this NpO_{2-x} phase has a configurational entropy term to account for the mixing of the (Np^{3+}) and (Np^{4+}) cations on the first sublattice, and (O^{2-}) or (Va) on the second sublattice.

Only the neutral member $(Np^{4+})(O^{2-})_2$ has a physical meaning, corresponding to stoichiometric NpO_2. The other three terms, namely $(Np^{4+})(Va)_2$ with a net charge of +4, $(Np^{3+})(O^{2-})_2$ with a net charge of −1, and $(Np^{3+})(Va)_2$ with a net charge of +3, are hypothetical and have a meaning only via electrically neutral combinations. A schematic representation of the model is given in Fig. 6. The neptunia phase, NpO_{2-x}, corresponds to a mixture of the four end members along the neutral line shown in bold in Fig. 6. One

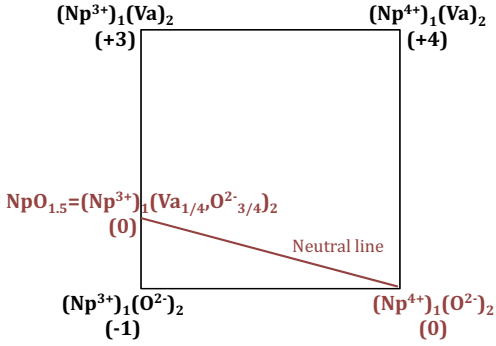

Fig. 6. Schematic representation of the sublattice model used to describe NpO_{2-x}, i.e., $(Np^{4+},Np^{3+})_1\ (O^{2-},Va)_2$.

endpoint of this line is NpO_2, the other one $NpO_{1.5}$. The completely reduced neptunia $NpO_{1.5}$ actually corresponds to the hypothetical neutral compound Np_2O_3(cr), or $(Np^{+3})(Va_{1/4}, O^{2-}_{3/4})_2$.

The Gibbs energies of the neutral members are expressed as follows:

$${}^{o}G_{NpO_2} = {}^{o}G_{(Np^{4+})_1(O^{2-})_2} \tag{22}$$

$${}^{o}G_{NpO_{1.5}} = \frac{1}{4}{}^{o}G_{(Np^{3+})_1(Va)_2} + \frac{3}{4}{}^{o}G_{(Np^{3+})_1(O^{2-})_2} + 2RT\left(\frac{1}{4}\ln\frac{1}{4} + \frac{3}{4}\ln\frac{3}{4}\right) \tag{23}$$

where ${}^{o}G_{NpO_2}$ is the Gibbs energy of NpO_2(cr), and ${}^{o}G_{NpO_{1.5}}$ the Gibbs energy of the hypothetical neutral compound Np_2O_3(cr).

We can express the Gibbs energies of $(Np^{4+})(Va)_2$ and $(Np^{3+})(Va)_2$ as:

$${}^{o}G_{(Np^{4+})_1(Va)_2} = {}^{o}G_{(Np^{4+})_1(O^{2-})_2} - 2{}^{o}G_O \tag{24}$$

$${}^{o}G_{(Np^{3+})_1(Va)_2} = {}^{o}G_{(Np^{3+})_1(O^{2-})_2} - 2{}^{o}G_O \tag{25}$$

where ${}^{o}G_O$ is the Gibbs energy of 1/2 O_2 gas.

Combining these four equations, one obtains the following expressions for the four end members:

$${}^{o}G_{(Np^{4+})_1(O^{2-})_2} = {}^{o}G_{NpO_2} \tag{26}$$

$${}^{o}G_{(Np^{4+})_1(Va)_2} = {}^{o}G_{NpO_2} - 2{}^{o}G_O \tag{27}$$

$${}^{o}G_{(Np^{3+})_1(Va)_2} = {}^{o}G_{NpO_{1.5}} - \frac{3}{2}{}^{o}G_O - 2RT\left(\frac{1}{4}\ln\frac{1}{4} + \frac{3}{4}\ln\frac{3}{4}\right) \tag{28}$$

$${}^{o}G_{(Np^{3+})_1(O^{2-})_2} = {}^{o}G_{NpO_{1.5}} + \frac{1}{2}{}^{o}G_O - 2RT\left(\frac{1}{4}\ln\frac{1}{4} + \frac{3}{4}\ln\frac{3}{4}\right) \tag{29}$$

The parameters assessed in the present model are those of ${}^{o}G_{NpO_{1.5}}$. The experimentally determined enthalpy and entropy values recommended by [14] were taken as initial parameters for the Gibbs energy function ${}^{o}G_{NpO_2}$. The heat capacity function of NpO_2 was taken from [19] and not optimized. As for the Gibbs energy of $NpO_{1.5}$, it was expressed as:

$${}^{o}G_{NpO_{1.5}} = 0.75{}^{o}G_{NpO_2} + 0.25{}^{o}G_{Np} + a + bT \tag{30}$$

where ${}^{o}G_{Np}$ is the Gibbs energy of Np(cr), and a and b are optimized parameters.

4.4. Liquid phase

The ionic two-sublattice model was used to describe the liquid phase [60], with Np^{4+} cations on the first sublattice, and O^{2-} anions, charged vacancies Va^{Q-}, and neutral oxygen O on the second sublattice:

$$(Np^{4+})_P(O^{2-}, Va^{Q-}, O)_Q \quad (31)$$

P and Q are equal to the average charge of the opposite sublattice:

$$Q = 4$$
$$P = 4y_{Va^{Q-}} + 2y_{O^{2-}} \quad (32)$$

where $y_{Va^{Q-}}$ and $y_{O^{2-}}$ are the site fractions of vacancies and divalent oxygen ions on the second sublattice. The induced charge of the vacancies corresponds to the average charge of the cation sublattice, i.e., $Q = 4$, while P varies with the composition via the site fractions $y_{O^{2-}}$ and $y_{Va^{Q-}}$ so as to keep the phase electrically neutral.

The Gibbs energy of the liquid phase is given by the following expression:

$$\begin{aligned} G^{liquid} =& y_{O^{2-}}\,{}^{o}G_{(Np^{4+})_2(O^{2-})_2} + y_{Va^{Q-}}\,{}^{o}G_{(Np^{4+})_1(Va^{1-})_4} + y_O\,{}^{o}G_O \\ &+ QRT(y_{O^{2-}}\ln y_{O^{2-}} + y_{Va^{Q-}}\ln y_{Va^{Q-}} + y_O \ln y_O) \\ &+ y_{O^{2-}}y_{Va^{Q-}}\left[L^0_{(Np^{4+})_P(O^{2-},Va^{Q-})_Q} + (y_{O^{2-}} - y_{Va^{Q-}})L^1_{(Np^{4+})_P(O^{2-},Va^{Q-})_Q}\right] \end{aligned} \quad (33)$$

${}^{o}G_{(Np^{4+})_2(O^{2-})_4}$, ${}^{o}G_{(Np^{4+})_1(Va^{1-})_4}$, and ${}^{o}G_O$ are the reference terms corresponding to the Gibbs energies of respectively neptunium dioxide NpO_2(l) (times two), pure neptunium, and pure oxygen. The Gibbs energy of the liquid phase also contains a configurational entropy term related to mixing of the species on the second sublattice. Finally, excess terms are expressed with the interaction parameters $L^0_{(Np^{4+})_P(O^{2-},Va^{Q-})_Q}$ and $L^1_{(Np^{4+})_P(O^{2-},Va^{Q-})_Q}$, which describe the liquid phase in the Np-NpO_2 composition range.

4.5. Gas phase

The gas phase was described by an ideal mixture of (Np, NpO, NpO_2, O, O_2, O_3) gaseous species. The Gibbs energy is expressed by:

$$G^{\varphi} = \Sigma y_i^o G_i^{\varphi} + RT\Sigma y_i \ln y_i + RT \ln P/P^o \quad (34)$$

where y_i is the fraction of the species i in the gas phase. ${}^{o}G_i^{\varphi}$ represents the standard Gibbs energy of the gaseous species i. P^o is the standard pressure. The O, O_2, and O_3 functions were taken from the SGTE database [61]. The Gibbs energy function for Np(g) was taken from the recent review by [13]. The entropy and heat capacity functions for NpO(g) and NpO_2(g) were taken from [14]. The enthalpies were those re-determined in this work as detailed Sections 2 and 3 (see Table 11).

5. Results and discussion

The optimized parameters of the liquid, NpO_{2-x}, and Np_2O_5 phases are listed in Table 8, and the calculated temperatures and phase compositions for invariant reactions are shown in Table 7 .

Table 7
Invariant reactions in the Np–O system.

Invariant reaction	T/K	Phase compositions, at.%O	Reference
L1 = NpO_{2-x} + γ-Np	913	γ-Np(0);NpO_{2-x}(66.667)	This work
L1 + L2 = NpO_{2-x}	1117	L1(0.055);NpO_{2-x}(41.2)	This work
Np_2O_5 = 2NpO_2 + 1/2O_2	700	71.428	This work
	700	71.428	[14]
$NpO_{1.90}$ = L	3069.5	65.49	This work
NpO_{2-x} + G = L	2879	NpO_{2-x}(66.33);L(67.20)	This work
NpO_{2-x} = L	3070 ± 62	66.667	[14,22]

5.1. Phase diagram

The calculated phase diagram is shown in Figs. 7 and 8 where it is compared with the available experimental data. The present model reproduces the main features as suggested by Richter and Sari [12]. One major difference, however, concerns the temperature of the monotectic reaction, calculated here at 1117 K, while Richter and Sari [12] reported it around 2450 K. The introduction of a miscibility gap around 2450 K was attempted, but found incompatible with both the oxygen potential data of Bartscher and Sari [24] and with the limit of the NpO_{2-x} domain towards hypostoichiometric compositions: either the miscibility gap and oxygen potential data could be reproduced, but the limit of the NpO_{2-x} domain could not; or the miscibility gap and limit of the NpO_{2-x} domain were both reproduced, but the oxygen potential data were no longer followed. The three data-sets appeared to be conflicting as presented in more detail in Appendix C. The oxygen potential data measured for neptunium dioxide are in fact consistent with NpO_{2-x} being in equilibrium with a liquid phase showing a high content of oxygen, and therefore with a monotectic invariant reaction found at lower temperatures. The increase of the monotectic temperature in the optimization routine produces a decrease of the oxygen content in the liquid phase in equilibrium with NpO_{2-x} and consequently a lowering of the oxygen potential data, which are no longer consistent with the experiment. The CALPHAD assessment presented by Kinoshita et al. [23] exemplifies this inconsistency, where the monotectic reaction is well-reproduced at 2450 K as well as the oxygen potential curves, but where the hypostoichiometric homogeneity range is far too extended. Complementary investigations of the liquidus line, of the existence of a miscibility gap, and of the temperature of the monotectic reaction are highly desirable.

The transition temperatures of the different allotropic forms of neptunium and the decomposition temperature of Np_2O_5(cr) are well described, as shown in Fig. 7. With the present model, the boundary between the single phase region NpO_{2-x}(cr) and the two phases region {NpO_{2-x}(cr)+Np(l)} is also in good agreement with the experimental points of Richter and Sari [12], obtained by Differential Thermal Analysis (DTA) from the thermal effects associated with the precipitation of neptunium metal. The DTA points at 2144 and 2265 K are particularly well followed. The hypostoichiometric range is slightly wider than suggested by the experimental data of Bartscher and Sari in the temperature range 1450–1950 K [24], but within the experimental uncertainties. It should be noted that the uncertainty on those phase boundary points, derived from their oxygen potential study combined with ceramographic and crystallographic analyses, is rather large. The extent of the NpO_{2-x} domain at those temperatures cannot be reduced more than presented without impairing the fitting to the oxygen potential data of Bartscher and Sari [24].

In addition, the melting point of neptunium dioxide is calculated at T_{fus} = 3069.5 K for congruently melting $NpO_{1.90}$, which is consistent with the recommended value at $T_{fus} = (3070 \pm 62)$ K [14,22]. The hypostoichiometric congruent melting composition is in accordance with the suggestions of [14].

5.2. Thermodynamic data of the neptunium oxide compounds

The entropy at 298.15 K and heat capacity function of NpO_2(cr) [14,19] were not optimized in this work. The calculated enthalpy of formation at 298.15 K (Table 9) is in excellent agreement with the recommended data [14]. The thermodynamic functions of Np_2O_5(cr) were optimized to fit the decomposition temperature of this compound as suggested by [12]. The calculated enthalpy, i.e., $-2172.0\ kJ \cdot mol^{-1}$, is in accordance with the recommended data [14], i.e., $\Delta_f H^o_m(Np_2O_5, cr, 298.15\ K) = -(2162.7 \pm 9.3)\ kJ \cdot mol^{-1}$.

Table 8
Summary of the thermodynamic data for pure elements and oxides selected in the present work. *SER* refers to the phase of the element stable at 298.15 K. The optimized coefficients are marked in bold.

Phase	Gibbs energy/(J·mol^{-1})	Reference
Liquid	${}^{o}G(Np^{4+})_2(O^{2-})_4$-$4{}^{o}H_O^{SER}$-$2{}^{o}H_{Np}^{SER}$ = $-$**1.8796083** × **10^6**+**570.0**T-132TlnT	This work + C_p from [14]
$(Np^{4+})_P(O^{2-},Va^{Q-},O)_Q$	${}^{o}G(Np^{4+})_1(Va^{1-})_4$-${}^{o}H_{Np}^{SER}$=$G_{Np}^{liq}$	[59]
	${}^{o}G_O$-${}^{o}H_O^{SER}$=G_O^{SER} − 2648.9 + 31.44T	[59]
	$L^0(Np^{4+})_P(O^{2-},Va^{Q-})_Q$ = **+392179–534.4**T	This work
	$L^1(Np^{4+})_P(O^{2-},Va^{Q-})_Q$ = −**330000**	This work
Gas	${}^{o}G_{Np}^{gas}$-${}^{o}H_{Np}^{SER}$=G_{Np}^{G}+RTln(10^{-5}P)	[14]
(Np,NpO,NpO_2,O,O_2,O_3)	${}^{o}G_{NpO}^{gas}$-${}^{o}H_{Np}^{SER}$-${}^{o}H_O^{SER}$ = G_{NpO}^{G}+RTln(10^{-5}P)	This work + [14]
	${}^{o}G_{NpO2}^{gas}$-${}^{o}H_{Np}^{SER}$-$2{}^{o}H_O^{SER}$ = G_{NpO2}^{G}+RTln(10^{-5}P)	This work + [14]
	${}^{o}G_O^{gas}$-${}^{o}H_O^{SER}$ = G_O^{G}+RTln(10^{-5}P)	[61]
	${}^{o}G_{O2}^{gas}$-$2{}^{o}H_O^{SER}$ = G_{O2}^{G}+RTln(10^{-5}P)	[61]
	${}^{o}G_{O3}^{gas}$-$3{}^{o}H_O^{SER}$ = G_{O3}^{G}+RTln(10^{-5}P)	[61]
NpO_{2-x}	${}^{o}G(Np^{3+})_1(O^{2-})_2$ − $2{}^{o}H_O^{SER}$ − ${}^{o}H_{Np}^{SER}$ = $G_{Np01.5}$+0.5G_O^{SER} + 1.12467RT	This work
$(Np^{3+},Np^{4+})(O^{2-},Va)_2$	${}^{o}G(Np^{4+})_1(O^{2-})_2$ − $2{}^{o}H_O^{SER}$ − ${}^{o}H_{Np}^{SER}$ = G_{NpO2}	This work + C_p from [19]
	${}^{o}G(Np^{3+})_1(Va)_2$ − ${}^{o}H_{Np}^{SER}$ = $G_{Np01.5}$ − 1.5G_O^{SER} + 1.12467RT	This work
	${}^{o}G(Np^{4+})_1(Va)_2$ − ${}^{o}H_{Np}^{SER}$ = G_{Np02} − 2G_O^{SER}	This work
Np_2O_5	G_{Np2O5} = −**2.2059589** × **10^6** + **451.36**T-99.2TlnT − 0.0493T^2	This work + C_p from [30]
Functions	G_{Np} = G_{Np}^{SER}	[59]
	G_O^{SER} = 1/2${}^{o}G_{O2}^{G}$	[59]
	G_{NpO2} = −**1.1019** × **10^6**+**409.09157**T − 71.608TlnT − .0079225T^2 + 450324T^{-1} (298 < T/K < 4000)	This work + C_p from [19]
	$G_{Np01.5}$ = 0.75G_{Np02} + 0.25G_{Np} **+ 1.525393** × **10^5** − **64.3**T (298 < T/K < 4000)	This work
	G_{Np}^{G} = 4.62305415 × 10^5−13.9440239T − 28.7334TlnT + 0.0206238T^2 − 1.27057833 × 10^{-5}T^3 +55670T^{-1}+3.820125 × 10^{-9}T^4−4.95395 × 10^{-13}T^5 (298 < T/K < 1400 K)	[13]
	G_{Np}^{G} = 4.18367996 × 10^5+287.602961T − 68.4689TlnT + 0.0243772T^2 − 4.73601667 × 10^{-6}T^3 +8054500T^{-1} + 5.09608333 × 10^{-10}T^4 − 2.2309 × 10^{-14}T^5 (1400 < T/K < 4000 K)	[13]
	G_{NpO}^{G} = −2.3537373 × 10^4 + 23.6932071T − 40.73102TlnT − 0.002534515T^2 − 9.31391667 × 10^{-7}T^3 +197552.5T^{-1}+2.71718333 × 10^{-10}T^4 (298 < T/K < 1400 K)	This work + [14]
	G_{NpO}^{G} = −3.72034191 × 10^4 + 117.398183T − 53.06105TlnT − 7.2306 × 10^{-4}T^2 + 3.2614 × 10^{-7}T^3 +2560795T^{-1} − 3.02156667 × 10^{-11}T^4 (1400 < T/K < 4000 K)	This work + [14]
	G_{NpO2}^{G} = −4.92292844 × 10^5 + 121.221111T − 56.33269TlnT − 0.020019715T^2 + 9.16285 × 10^{-6}T^3 +366402.5T^{-1} − 1.91906917 × 10^{-9}T^4 (298 < T/K < 1000 K)	This work + [14]
	G_{NpO2}^{G} = −4.93581448 × 10^5 + 188.906305T − 68.29804TlnT + 0.004517016T^2 − 9.09885833 × 10^{-7}T^3 +185016.85T^{-1} − 5.52373 × 10^{-11}T^4 (1000 < T/K < 4000 K)	This work + [14]

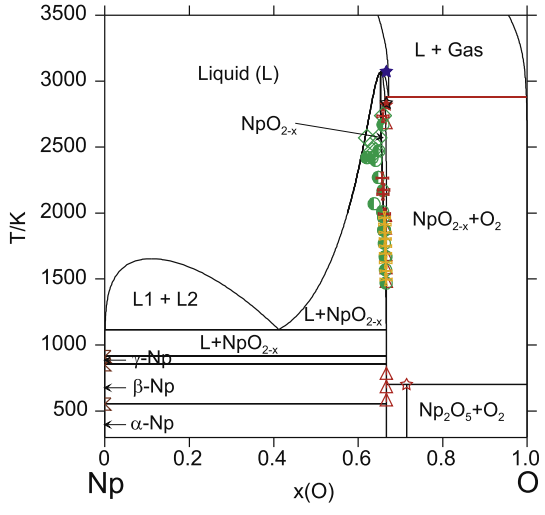

Fig. 7. Calculated phase diagram for Np–O at 1 bar.

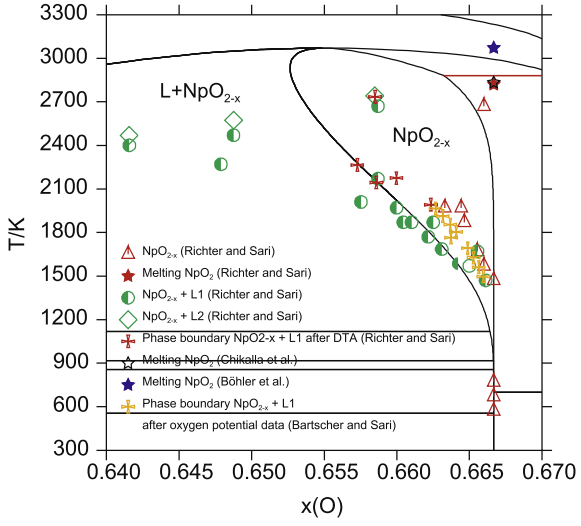

Fig. 8. Calculated phase diagram for Np–O at 1 bar, and comparison with the experimental data.

The entropy value is in strong disagreement with the selected data, however. The adjustment to $S_m^o(Np_2O_5, cr, 298.15K) = 242.4\ J \cdot K^{-1} \cdot mol^{-1}$ appeared necessary to meet the decomposition temperature at about 700 K as reported by Richter and Sari [12]. But this decomposition temperature is not well known and needs further experimental investigations. The recommended entropy value, which was actually never measured experimentally, but estimated

Table 9
Calculated thermodynamic data for the neptunium oxide compounds, and comparison with literature data.

Phase	$\Delta_f H^o_m$ (298.15 K) ($kJ \cdot mol^{-1}$)	S^o_m (298.15 K) ($J \cdot K^{-1} \cdot mol^{-1}$)	Reference
NpO_2(cr)	−1076.8	80.3	This work
	−1078.5 ± 2.7	80.3 ± 0.4	[14]
Np_2O_5(cr)	−2172.0	242.4	This work
	−2162.7 ± 9.3	186 ± 15	[14]

by Merli and Fuger as $S^o_m(Np_2O_5, cr, 298.15\ K) = (186 \pm 15)\ J \cdot K^{-1} \cdot mol^{-1}$ [14,29], leads to a decomposition temperature at 236 K. The equilibrium decomposition temperature for reaction (35) is directly related to the values of the thermodynamic functions for NpO_2(cr), Np_2O_5(cr) and O_2(g). This inconsistency shows that one of the functions must be ill-defined, most probably the entropy and/or heat capacity of Np_2O_5, or the decomposition temperature, which should be re-assessed.

$$Np_2O_5(cr) = 2NpO_2(cr) + O_2(g) \quad (35)$$

The heat capacity data of NpO_2(cr) were not optimized in the present model, but taken from Beneš et al. [19]. Looking at the calculated Np–O phase diagram in Fig. 8, one can see that neptunium dioxide starts to loose oxygen at about 1800 K, and becomes substoichiometric. The heat capacity function shown in Fig. 9a calculated at the composition x(O)=0.66667, i.e., corresponding to O/Np = 2, was derived two different ways: one excludes the gas phase from the calculation, the other includes it to account for the equilibrium between NpO_{2-x}(cr) and O_2(g) at the composition x(O)=0.66667, as depicted in Fig. 8. If the gas phase is excluded when performing the calculation, the derived heat capacity is the one of Beneš et al. [19]. It has a lattice contribution only (Fig. 9a). If the gas phase is considered in equilibrium with NpO_{2-x}(cr), the calculated heat capacity function shows an increase above about 1850 K, which can be attributed to the departure from stoichiometry and formation of oxygen vacancies. This feature is also illustrated by the defect fractions of Np^{3+} cations and vacancies which augment on the first and second sublattices, respectively, as the temperature is increased (Fig. 9b).

Konings and Beneš have predicted the existence of an excess heat capacity, but of different nature [20]. The authors have suggested the presence of an excess component in stoichiometric NpO_2 due to defect formation, and more exactly due to the formation of oxygen Frenkel pairs, by analogy with the heat capacity functions of ThO_2, UO_2, and PuO_2 [20] as mentioned in Section 2.1. The corresponding excess heat capacity is shown in Fig. 9a. Oxygen Frenkel pairs cannot be described with the present model, as oxygen interstitials are not taken into account in the sublattice model. But it is interesting to point out that both effects, i.e., departure from stoichiometry at those high temperatures, and oxygen Frenkel pairs formation in stoichiometric NpO_2, could contribute to the extent of an excess component. Experimental heat capacity or enthalpy increment measurements above 1800 K are required to confirm the existence of this excess component, and for a thorough investigation of the underlying mechanisms.

5.3. Oxygen chemical potential of NpO_{2-x}

The oxygen potential curves derived with the model at 1473, 1573, 1673, 1773, and 1853 K, are in good agreement with the experimental data of Bartscher and Sari [24]. The corresponding variation of the constituent fractions on the first and second sublattices as a function of O/Np ratio is shown in Fig. 10b at 1853 K. As expected, the fractions of Np^{3+} cations and vacancies augment as the phase becomes more reduced.

5.4. Vapourization behaviour

The Np(g), NpO(g), NpO_2(g), O(g), O_2(g), and O_3(g) partial pressures calculated with the model for the azeotropic composition NpO_{2-x} are shown in Fig. 11, together with the present mass spectrometry data, those of Ackermann et al. over quasi-stoichiometric neptunium dioxide (300 mg sample), and Gotcu-Freis et al. under vacuum. The total pressures derived with the model are in very good agreement with our experimental data and that of Gotcu-Freis et al., but slightly higher than measured by Ackermann et al. The Np(g), O_2(g), and O_3(g) partial pressures are found several orders of magnitude lower, in good accordance with the experiment. The calculated azeotropic vapour composition at 2260 K is: 93.2% NpO_2(g), 6.1% NpO(g), and 0.7% O(g), which corresponds to an oxygen-to-metal ratio $(O/Np)_{azeotropic} = (1.945 \pm 0.003^1)$ at 2260 K.

The partial pressures obtained under vacuum in the work of Gotcu-Freis et al. (93% NpO_2(g), 6% NpO(g), and 1% Np(g) at 2260 K) and in the present study (85.2% NpO_2(g) and 14.8% NpO

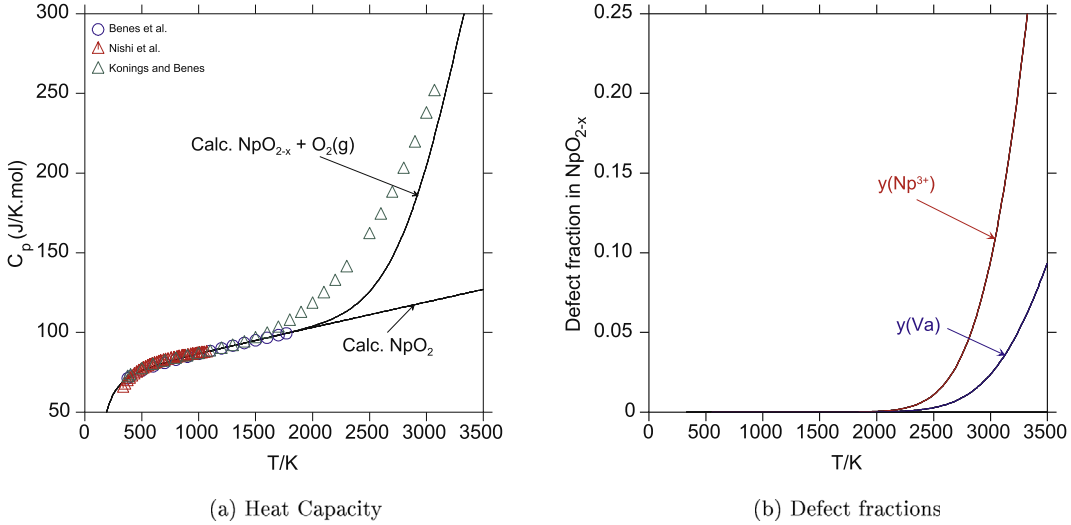

(a) Heat Capacity (b) Defect fractions

Fig. 9. (a) Calculated heat capacity at the composition x(O) = 0.66667 and (b) defect fractions as a function of temperature.

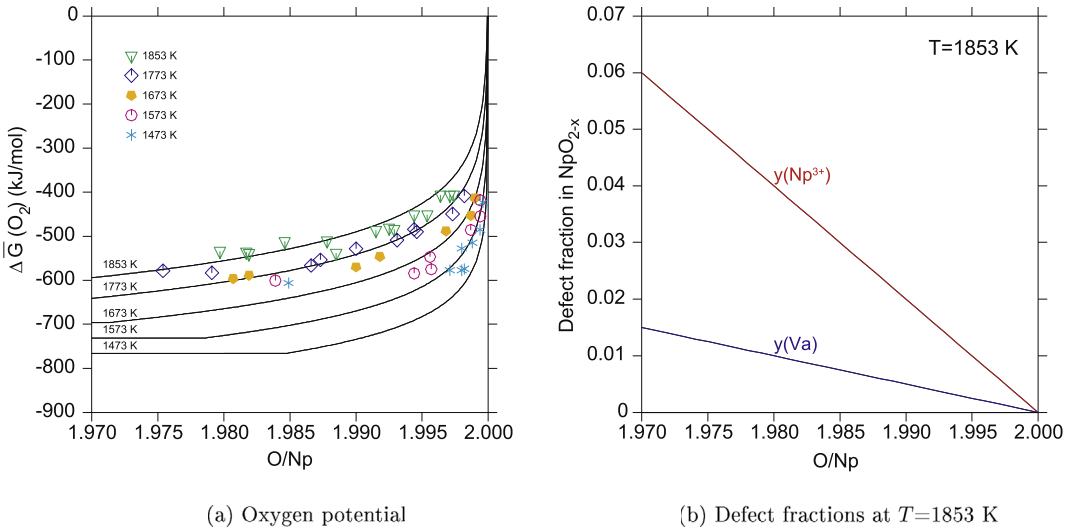

(a) Oxygen potential (b) Defect fractions at T=1853 K

Fig. 10. (a) Calculated oxygen potential in NpO_{2-x} together with the experimental data of Bartscher and Sari [24]. (b) Calculated fraction of defects in NpO_{2-x} as a function of composition at 1853 K.

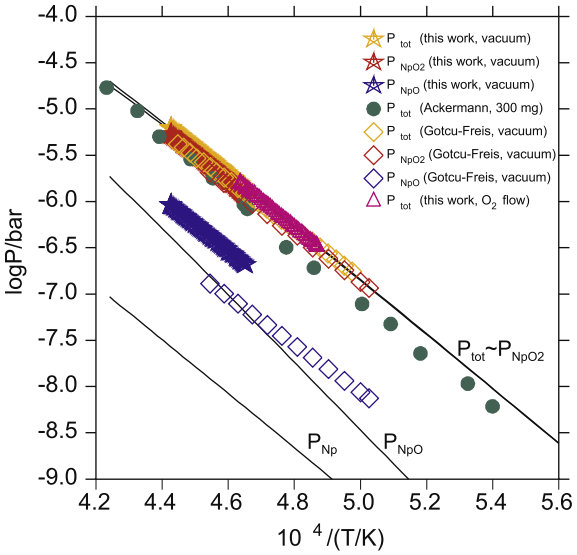

Fig. 11. Calculated total pressure and partial pressures of Np(g), NpO(g), NpO_2(g), O(g), O_2(g), and O_3(g) versus reciprocal temperature for the azeotropic composition NpO_{2-x}, and comparison with the present mass spectrometry study, and data of Ackermann et al. [10] and Gotcu-Freis et al. [11] (1 bar = 100 kPa).

(g) at 2262 K), are plotted in Fig. 11. As detailed in Section 3.2 and reported in Table 10, this corresponds to an O/Np ratio in the gas phase equal to $(O/Np)_{gas} = (1.967 \pm 0.003^{1})$ and (1.856 ± 0.003^{1}), respectively, considering the contributions of O(g) and O_2(g) estimated from the equilibrium between NpO(g)/NpO_2(g) and O(g)/O_2(g). Our thermodynamic model shows that the O(g) partial pressure contribution should be quite significant close to stoichiometric NpO_2 and congruently vaporizing NpO_{2-x}. The experimental limitations of the KEMS measurement, namely the high background level at low masses, therefore introduce a rather large uncertainty on the determination of the O/Np ratio in the gas phase.

One way to assess the O/Np ratio of the solid phase, and thereafter of the gas phase supposing that the congruent composition is reached during the experiment, is to quench the investigated material after the Knudsen experiment, and to perform a post-analysis of the stoichiometry of the solid using a thermogravimetry technique. In the present work, the amount of material left after quenching was unfortunately too small (of the order of 30–40 mg) to carry out such an analysis. Instead, the solid composition, which is listed in Table 10, was assessed using the equilibrium reaction (9) between NpO(g) and NpO_2(g) gaseous species combined with our thermodynamic model following the method described in detail by Beneš et al. [52]. The equilibrium partial pressure of oxygen P_{O_2} was firstly calculated from the vapour pressures of the Np bearing species as described in Section (3.2) based on Eqs. (9), (11) and (12). The corresponding oxygen potential over solid neptunia was thereafter derived using Eq. (36), and the composition of the NpO_{2-x} solid phase was estimated from the $\Delta\overline{G}(O_2) = f(O/Np)_{solid}$ curves calculated from the thermodynamic model.

Table 10
Assessment of the (O/Np) ratios in the gas and solid phases based on the experimental KEMS data, and comparison with the calculated azeotropic and congruent compositions using the present CALPHAD model. [a] Data calculated using $\Delta_f H^o_m(NpO,g,298.15\ K) = -16.6\ J \cdot K^{-1} \cdot mol^{-1}$. [b] Data calculated using $\Delta_f H^o_m(NpO,g,298.15\ K) = -9.8\ J \cdot K^{-1} \cdot mol^{-1}$.

	T[c]/K	Vapour composition (KEMS data)	$(O/Np)^d_{gas}$	$(O/Np)^d_{solid}$
KEMS data				
This work	2262	85.2%NpO_2(g) + 14.8%NpO(g)	1.856	1.918[b]
Gotcu-Freis et al.	2260	93%NpO_2(g) + 6%NpO(g) + 1%Np(g)	1.967	1.939[b]
CALPHAD model				
Closed system A	2260	93.2%NpO_2(g) + 6.1%NpO(g) + 0.7%O(g)	1.945[a]	1.945[a]
Closed system B	2260	92.9%NpO_2(g) + 6.7%NpO(g) + 0.4%O(g)	1.937[b]	1.937[b]
Open system B	2260	91.8%NpO_2(g) + 7.9%NpO(g) + 0.4%O(g)	1.933[b]	1.933[b]

[c] Standard uncertainties u are $u(T) = 10$ K.
[d] Standard uncertainties u are $u(O/Np) = 0.003$.

Table 11
Thermodynamic data for the neptunium gaseous species used in the present thermodynamic model.

Phase	$\Delta_f H^o_m(298.15\ K)/(kJ \cdot mol^{-1})$	Ref.	$S^o_m(298.15\ K)/(J \cdot K^{-1} \cdot mol^{-1})$	Ref.
Np(g)	470 ± 5	[13]	197.72 ± 0.10	[13]
NpO(g)	−9.8 ± 7.8[a]	This work	253.060 ± 4.0	[14]
NpO_2(g)	−471.7 ± 3.3[a]	This work	269.892 ± 6.0	[14]

[a] The quoted uncertainties are standard uncertainties.

$$\Delta\bar{G}(O_2)(T/K) = R(T/K)\ln P_{O_2} = 2RT\ln\left(\frac{P_{NpO_2}}{P_{NpO}K_P}\right) \quad (36)$$

The latter calculation yielded an oxygen-to-metal ratio $(O/Np)_{solid} = (1.918 \pm 0.003)$[3] in the present work, and $(O/Np)_{solid} = (1.939 \pm 0.003)$[3] when applied to the data of Gotcu-Freis et al. (see Table 10).

The calculated $(O/Np)_{solid}$ compositions based on this work and that of Gotcu-Freis et al. are found below the azeotropic composition. Such stoichiometries should not be reached when starting from a stoichiometric $NpO_{2.0}$ sample. It is therefore likely that our model slightly overestimates the azeotropic vapour composition. A number of reasons can explain this discrepancy.

5.4.1. NpO(g) and NpO_2(g) thermodynamic data

The calculated composition at azeotropic vapourization is directly related to the values of the thermodynamic functions for NpO(g) and NpO_2(g) (see Table 11). The enthalpy of formation of NpO_2(g) has been carefully re-examined in this work, and can be retained with a reasonable degree of confidence. The enthalpy of formation of NpO(g) recommended in the review by Konings et al. [14] has been derived from the mass spectrometric measurements of Ackermann and Rauh on the two isomolecular reactions NpO(g) + La(g) = Np(g) + LaO(g) and Np(g) + YO(g) = NpO(g) + Y(g), respectively [37]. The accuracy of the derived result depends on the accuracy of the former assessment of the thermodynamic functions of the reference compounds La(g), LaO(g), Y(g), and YO(g). The latter have been estimated in the literature using Knudsen effusion and mass spectrometry methods at a low value of the ionization potential to avoid fragmentation processes [55,62]. Such a determination at low energies introduces rather large uncertainties, however, as the absolute and relative ionization cross sections tabulated in the literature are usually accurate only at the maximum ionization energy, when considering the totality of the ionization process (parent and fragment ions) [55].

Younès has suggested a new method to circumvent this problem, and therefore to derive a more reliable result [63]. The author firstly assessed the fragmentation processes of LaO(g) and YO(g) species by measuring their full ionization patterns [63]. Using these data, [63] subsequently corrected the intensity values published in the literature at low ionization energies, and derived the corresponding values at maximum of the ionization cross sections [55,62,63]. In addition, Younès estimated the ratio of maximum ionization cross sections for Y/YO and La/LaO based on mass spectrometric measurements rather than using the additivity rule of Otvos and Stevenson [50], which has shown limitations for oxides [42], i.e., $\sigma_Y/\sigma_{YO}(max) = 1.5$ and $\sigma_{La}/\sigma_{LaO}(max) = 1.67$ [62,63]. Using both corrections (for the ionic intensities and cross sections at the voltage for maximum ionization cross section), Younès re-evaluated the published data, and derived enthalpies of formation as $\Delta_f H^o_m(LaO, g, 298.15\ K) = -(114.2 \pm 8.4)\ kJ \cdot mol^{-1}$ and $\Delta_f H^o_m(YO, g, 298.15\ K) = -(40.12 \pm 9.9)\ kJ \cdot mol^{-1}$, respectively.

In the present work, the enthalpy of formation of NpO(g) has been re-evaluated using the data of Ackermann and Rauh [37] combined with the reference functions for La(g), LaO(g), Y(g) and YO(g) as reported in the work of Younès [62,63] and Heyrman et al. [55] as the latter data are considered more reliable. The detail of this calculation is given in Appendix B. The value retained in this work based on third law analysis is $\mathbf{\Delta_f H^o_m(NpO, g, 298.15\ K) = -(9.8 \pm 7.8^1)\ kJ \cdot mol^{-1}}$ (Table 11).

The use of this function instead of the one recommended by [14], i.e., $\Delta_f H^o_m(NpO, g, 298.15\ K) = -(16.6 \pm 10.0)\ kJ \cdot mol^{-1}$, leads to a slightly more reduced composition at azeotropic vapourization, i.e., 92.9%NpO_2(g) + 6.7%NpO(g)+0.4%O(g), corresponding to an oxygen-to-metal ratio $(O/Np)_{azeotropic} = (1.937 \pm 0.003^1)$ at 2260 K. The agreement between the CALPHAD model and the experimental results is therefore slightly improved. The azeotropic compositions calculated at this same temperature with the model of [2] for urania and plutonia are $(O/U)_{azeotropic} = (1.991 \pm 0.003)$ and $(O/Pu)_{azeotropic} = (1.911 \pm 0.003)$, respectively. The trend of decreasing stability along the series U–Np–Pu is in good accordance with the corresponding trends in oxygen potential data.

The standard entropies and heat capacities of both gaseous species NpO(g) and NpO_2(g) were derived using estimated molecular parameters [14], as there are unfortunately no experimental data available on the molecular structures and spectra of these molecules. This introduces a quite large degree of uncertainty on those functions, and therefore a similarly large uncertainty on the azeotropic composition calculated with the model.

A very good agreement between second and third law analyses was found in the present mass spectrometry studies when determining the sublimation enthalpy of NpO_2(cr). The reported standard entropy for NpO_2(g) should hence be retained. The discrepancy could therefore originate from a poorly defined standard entropy of the NpO(g) species. A lower entropy value would lead to a more reduced azeotropic composition, in better agreement with our experimental results. We did not re-adjust this entropy data in the model, however, to stay consistent with the third law analysis of the enthalpy of formation of NpO(g). Our results point, however, to the need to re-evaluate the entropy and heat capacity functions of NpO(g).

5.4.2. Azeotropic versus congruent vapourization

The calculated composition at azeotropic vapourization refers to a closed system and to the state where gas and condensed phases have the same composition [55]. Knudsen effusion cell measurements correspond to open systems, however, as opposed to closed ones, where the azeotropic definition is substituted for a congruent flow relation. The O/Np ratio of the solid phase is then equal to the atomic flow ratio in the gas phase as expressed in Eq. (8) [55]. As shown in Fig. 12, the calculated composition at congruent vapourization (see Appendix A for further details on the calculation) yields, for a given temperature, slightly lower values than the corresponding azeotropic composition. We obtain $(O/Np)_{congruent} = (1.933 \pm 0.003^1)$ at 2260 K.

5.4.3. Shape of the total pressure curve

The total and partial pressures calculated with the present model for a closed system at 2262 K are shown in Fig. 13 as a function of O/Np ratio of the solid phase. The total pressure denoted

[3] Data calculated using $\Delta_f H^o_m(NpO, g, 298.15\ K) = -9.8\ J \cdot K^{-1} \cdot mol^{-1}$ as selected in this work. The quoted uncertainty corresponds to the standard uncertainty.

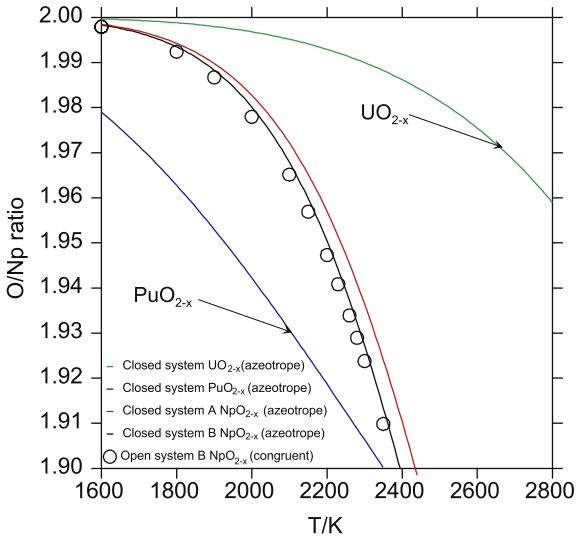

Fig. 12. Congruent composition calculated with the present model as a function of temperature using the azeotrope (closed system), and atomic flow (open system) ratio definitions.

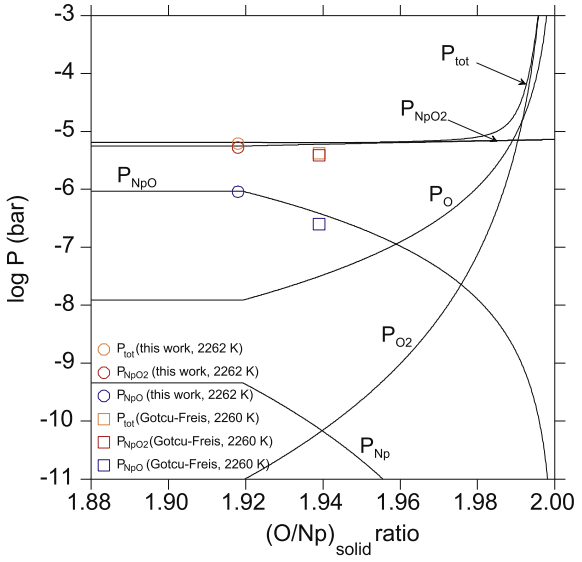

Fig. 13. Variation of the total and partial pressures versus O/Np ratio at 2262 K for a closed system as calculated with the CALPHAD model, and comparison with experimental data. The calculated P_{tot}(bar) corresponds to P_{tot}(bar) = P(Np) + P(NpO) + P(NpO_2) + P(O) + P(O_2)+P(O_3) (1 bar = 100 kPa).

{P_{tot}} refers to the sum of partial pressures for neptunium and oxygen bearing species, i.e., $\{P_{Np} + P_{NpO} + P_{NpO_2} + P_O + P_{O_2} + P_{O_3}\}$. The azeotropic composition corresponds to the minimum in the latter total pressure curve. The severe flatness of the total pressure curve around the minimum is worth pointing out, as it introduces a quite large degree of uncertainty on the exact value of the composition at congruent vapourization derived from the model. This feature is more pronounced than in the U–O and Pu–O systems [7].

The calculated NpO_2(g) contribution is quasi unchanged throughout the whole composition range, in accordance with the experimental observations [10,11]. When heating neptunium dioxide at this temperature under vacuum, the system preferentially releases O(g) and O_2(g), driving to the sample's reduction until the congruent vapour composition is reached. No more reduction should occur beyond this point. Starting from a more reduced

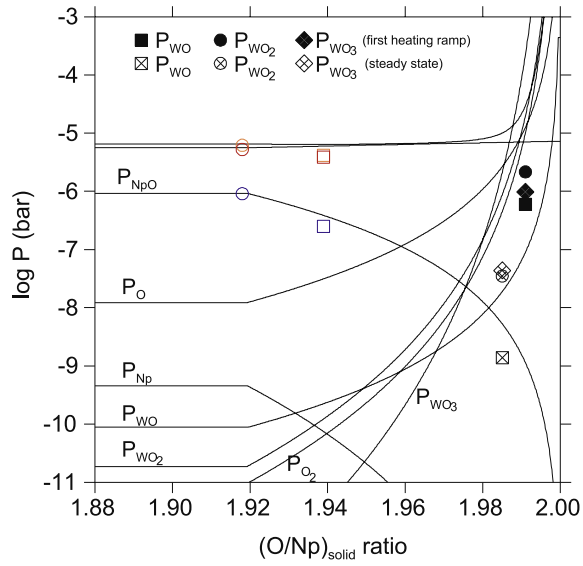

Fig. 14. Variation of the total and partial pressures versus O/Np ratio of the condensed phase at 2262 K for a closed system when W is present, and comparison with experimental data (1 bar = 100 kPa).

composition than $(O/Np)_{congruent}$, the sample oxidizes up to the congruent composition through a preferential loss of NpO(g).

5.4.4. Tungsten influence

One might finally argue that the tungsten cell material plays a role in the sample reduction. This has to be nuanced, however. Signals of WO(g), WO_2(g), and WO_3(g) were indeed detected in our experiments during the initial heating stage under vacuum, but decreased to background level during the temperature plateau. If the W material would enhance the reduction, it should not result in a change below congruent composition. Partial pressures were recalculated with the model at 2262 K, when introducing W into the system, and are shown in Fig. 14. The congruent point is not changed in this calculation, nor the shape and absolute values of neptunium bearing species although W is present in the system. The calculated partial pressures of the gaseous tungsten oxides reach significant values close to the $NpO_{2.0}$ composition nevertheless, which is why we could observe them experimentally. The partial pressures of the gaseous tungsten oxides recorded in the experiment are of the same order of magnitude as the ones calculated for $NpO_{1.991}$(cr). After a few hours of stabilisation, those partial pressures reach the level of $NpO_{1.985}$(cr), and are then hardly detectable.

Future studies of the congruent state should consider performing the mass spectrometry measurements in an iridium cell instead of tungsten so as to avoid the formation of parasite tungsten oxide species. The detection of O_2(g) and O(g) species might become possible in such a cell. In addition, those studies should ideally be performed with large amounts of material (in the order of 300 mg instead of the few tens of milligrams used here) in an attempt to obtain an independent analysis of the O/Np ratio with a post measurement of the solid phase by thermogravimetry. Nevertheless, based on the present experimental results and CALPHAD model, we can estimate the composition at congruent vapourization at 2260 K as (O/Np) = (1.92 ± 0.01[1]). The (O/Np) ratio determined experimentally is probably slightly underestimated due to limitations in the measurement of the O(g) and O_2(g) partial pressures by KEMS, while the CALPHAD model probably overestimates this value slightly due to ill-defined entropy and heat capacity data for NpO(g). Further experimental investigations of the thermody-

namic functions of NpO(g) are needed for a better description of the system.

6. Conclusions

Knudsen effusion mass spectrometry measurements have provided in the present work a better insight into the vapourization behaviour of neptunium dioxide. The enthalpy of formation of NpO_2(g) has been re-assessed with measurements under oxygen flow and derived as $\Delta_f H^o_m(\mathbf{NpO_2}, \mathbf{g}, \mathbf{298.15\ K}) = -(\mathbf{471.7 \pm 3.3}^{1})$ $\mathbf{kJ \cdot mol^{-1}}$, i.e., about 15 $kJ \cdot mol^{-1}$ lower than the value selected in the literature [10,14]. A thermodynamic model for the Np–O system has also been reported using the CALPHAD method, which is consistent with the experimental data available in the literature. The substoichiometric domain NpO_{2-x} and liquid phase have been described using the compound energy formalism and ionic two-sublattice model, respectively, as was previously done for the U–O [5] and Pu–O [6] systems. The main features of the Np–O binary phase diagram – boundary line between the single phase NpO_{2-x} and two-phases domain {NpO_{2-x}+Np(l)}, melting temperatures of neptunium metal and neptunium dioxide, miscibility gap in the metal rich part, decomposition temperature of Np_2O_5(cr), transition temperatures of the different allotropic forms of Np(cr) – are well reproduced. In addition, the calculated oxygen chemical potentials over NpO_{2-x} are in good agreement with the literature. The temperature of the monotectic reaction is lower than suggested in the literature, however. The oxygen potential data reported on this system were found incompatible with NpO_{2-x} being in equilibrium with a liquid phase with a low content of oxygen, and therefore with a higher monotectic temperature. The total pressures derived with the model at azeotropic vapourization, and for a given temperature as a function of O/Np ratio of the NpO_{2-x}(cr) solid phase, are consistent with the present Knudsen effusion mass spectrometry measurements and data of Ackermann et al. [10] and Gotcu-Freis et al. [11]. The azeotropic and congruent compositions, applicable to closed and open systems, derived from the CALPHAD model are O/Np = (1.937 ± 0.003^{1}) and (1.933 ± 0.003^{1}), respectively, which are probably slightly overestimated. The discrepancy with the experimental results have pointed to the need for a re-assessment of the thermodynamic functions of NpO(g). The enthalpy of formation has been re-calculated based on the data of Ackermann and Rauh [37]: the selected value is $\Delta_f H^o_m(\mathbf{NpO}, \mathbf{g}, \mathbf{298.15\ K}) = -(\mathbf{9.8 \pm 7.8}^{1})$ $\mathbf{kJ \cdot mol^{-1}}$. Finally, based on the experimental information combined with the CALPHAD model, the composition at congruent vapourization at 2260 K has been estimated as $(\mathbf{O/Np}) = (\mathbf{1.92 \pm 0.01}^{1})$, which is in good accordance with the trend of decreasing stability along the series U–Np–Pu.

This study has finally highlighted a number of missing or poorly described experimental points, that should be re-assessed for a better description of the neptunium–oxygen system:

- investigation of the liquidus line in the whole phase diagram, and especially of the possible existence of a miscibility gap;
- examination of the temperature of the corresponding monotectic reaction and extent of the miscibility gap;
- determination of the oxygen solubility limits in Np(cr) and Np (l);
- complementary oxygen potential measurements over NpO_{2-x}(cr) at higher temperatures, as well as high temperature X-ray diffraction measurements under controlled atmosphere (meaning under known oxygen potential conditions) to better define the extent of the NpO_{2-x}(cr) hypostoichiometric domain;
- assessment of the relationship between liquidus temperature and composition of the NpO_{2-x}(cr) phase, and especially determination of the (O/Np) ratio of the congruently melting composition (although this seems to be extremely challenging as such information is probably not accessible with the current experimental facilities [22]);
- Knudsen effusion mass spectrometry measurements on large amounts of neptunium dioxide material (~300 mg) in iridium cells with a post determination of the solid phase composition after heating at a given temperature.
- re-assessment of the thermodynamic functions of NpO(g), as the large associated uncertainties introduce a similarly large uncertainty on the congruent composition calculated with the CALPHAD model.

The refined parameters reported herein provide a sound basis for the modelling of the Np–O system and higher oxide systems that can be re-visited as complementary measurements become available.

Acknowledgements

The authors would like to express their gratitude to D. Bouëxière for the collection of the X-ray diffraction data. The authors also thank Dr. C. Chatillon for the very fruitful discussions. ALS acknowledges the European Commission and the Ras al Khaimah Centre for Advanced Materials for funding her PhD studentship. This research contributes to the joint programme on nuclear materials (JPNM) of the European Energy Research Alliance (EERA).

Appendix A. Congruent flow calculation with Thermo-calc: description of the method

The congruent flow calculation was performed using the module "PARROT" of the Thermo-calc software, whose least-squares optimization procedure is described in detail in [64].

The goal of the optimization procedure is to scan, for a given temperature, through a range of oxygen potentials until one specific oxygen potential is found, where the congruent flow relation is satisfied, i.e., where the (O/Np) ratio of the solid NpO_{2-x} phase is equal to the atomic flow ratio in the gas phase in equilibrium with it:

$$\Delta = (O/Np)_{NpO_{2-x}} - F_O^{gas}/F_{Np}^{gas} = 0 \tag{A.1}$$

The (O/Np) ratio of the solid NpO_{2-x} phase is simply expressed by the ratio of the atomic molar fractions in this phase $x_O^{NpO_{2-x}}$ and $x_{Np}^{NpO_{2-x}}$:

$$(O/Np)_{NpO_{2-x}} = x_O^{NpO_{2-x}}/x_{Np}^{NpO_{2-x}} \tag{A.2}$$

The atomic flows between oxygen and neptunium, F_O^{gas} and F_{Np}^{gas}, are expressed as a function of temperature, partial pressure, and molar mass of the species vaporizing using the appropriate Hertz-Knudsen relations [53–55] according to:

$$F_O^{gas} = sC/(2\pi RT)^{1/2} \cdot \left[P_O/(M_O)^{1/2} + P_{NpO}/(M_{NpO})^{1/2} + 2P_{NpO_2}/(M_{NpO_2})^{1/2} + 2P_{O_2}/(M_{O_2})^{1/2}\right] \tag{A.3}$$

$$F_{Np}^{gas} = sC/(2\pi RT)^{1/2} \cdot \left[P_{Np}/(M_{Np})^{1/2} + P_{NpO}/(M_{NpO})^{1/2} + P_{NpO_2}/(M_{NpO_2})^{1/2}\right] \tag{A.4}$$

where s is the area of the effusion orifice, C the Clausing factor, M_i the molar mass, P_i the partial pressure, T the temperature, and R the universal gas constant equal to 8.314472 $J \cdot K^{-1} \cdot mol^{-1}$.

"PARROT" is used to optimize the oxygen potential above the NpO_{2-x} phase until the value of Δ reaches zero, and the calculated values of $(O/Np)_{NpO_{2-x}}$ and F_O^{gas}/F_{Np}^{gas} are equal.

Appendix B. Re-assessment of the enthalpy of formation of NpO(g)

In the present work, the enthalpy of formation of NpO(g) has been re-evaluated using the data of Ackermann and Rauh [37] combined with the reference functions for La(g), LaO(g), Y(g) and YO(g) as reported in the work of Younès [62,63] and Heyrman et al. [55] (listed in Tables B.1 and B.2) as the latter data are considered more reliable. The entropy and heat capacity functions listed in Tables B.1 and B.2 have been derived using the rotational, vibrational, and electronic molecular parameters of the gas species listed in the papers of [55,13]. The thermodynamic functions for Np(g) have been taken from the review by Konings et al. [13].

The Knudsen effusion mass spectrometry measurements of Ackermann and Rauh have been performed using La(cr), La_2O_3(cr), Y(cr), and Y_2O_3(cr) together with Np(cr) in a tungsten cup and molybdenum cell at 10.5 eV ionization energy to avoid fragmentation of the LaO(g) molecule [37]. The associated equilibrium reactions (A.5) and (A.6) and the measured reaction enthalpies are listed in Table B.3. The corresponding equilibrium constants are expressed by the relations (A.7) and (A.8):

$$NpO(g) + La(g) = Np(g) + LaO(g) \quad (A.5)$$

$$Np(g) + YO(g) = NpO(g) + Y(g) \quad (A.6)$$

$$K_{p,A} = K_A^+ \Sigma_A = \left(\frac{I_{Np}^+ I_{LaO}^+}{I_{NpO}^+ I_{La}^+}\right)\left(\frac{\sigma_{NpO}\sigma_{La}}{\sigma_{Np}\sigma_{LaO}} \cdot \frac{f_{NpO} f_{La}}{f_{Np} f_{LaO}} \cdot \sqrt{\frac{M_{Np} M_{LaO}}{M_{NpO} M_{La}}}\right) \quad (A.7)$$

$$K_{p,B} = K_B^+ \Sigma_B = \left(\frac{I_{NpO}^+ I_{Y}^+}{I_{Np}^+ I_{YO}^+}\right)\left(\frac{\sigma_{Np}\sigma_{YO}}{\sigma_{NpO}\sigma_{Y}} \cdot \frac{f_{Np} f_{YO}}{f_{NpO} f_{Y}} \cdot \sqrt{\frac{M_{NpO} M_{Y}}{M_{Np} M_{YO}}}\right) \quad (A.8)$$

where I_{Np}^+, I_{NpO}^+, I_{La}^+, I_{LaO}^+, I_Y^+ and I_{YO}^+ are the measured intensities for the Np(g), NpO(g), La(g), LaO(g), Y(g) and YO(g) vapour species, σ_i their ionization cross sections, f_i their isotopic abundance, and M_i their molar masses.

Ackermann and Rauh have used the data of Mann at maximum of the ionization cross sections to estimate the equilibrium constants of reaction, although their measurements were done at 10.5 eV [37]. The authors did not report individual intensity values for the ionic vapour species unfortunately, so that a correction based on the method of Younès was not possible. Instead, the cross section values have been corrected to match an ionization energy of 10.5 eV using the program SIGMA [42,47,48] and the additivity rule for the molecular species, yielding $\Sigma_A = 1.02209$ and $\Sigma_B = 0.95115$.

Using the aforementioned corrections, the data of Ackermann and Rauh [37] were subsequently re-analyzed in this work by second and third law methods. The enthalpy of reaction at the median temperature was assigned an uncertainty of ($\pm 4\ \mathrm{kJ \cdot mol^{-1}}$) for the second law calculation. As Ackermann and Rauh did not report any absolute values for the partial pressures, but only their least-squares fitted equations $\log K^+$, the third law was applied using the end and median temperatures for each temperature interval. The results of our calculations are listed in Table B.3.

For both isomolecular reactions, second and third laws are in good agreement within the experimental uncertainties. The results obtained for the equilibrium with the lanthanum species are more positive than those obtained with the yttrium species, however. Based on the reported data, it is not possible to discard one set of experiments. The weighted mean values obtained from both sets of experiments are $\Delta_f H_m^o(\mathrm{NpO, g, 298.15\ K}) = -(9.3 \pm 8.3)\ \mathrm{kJ \cdot mol^{-1}}$

Table B.1
Summary of the standard formation enthalpy and entropy for La(g), LaO(g), Y(g), and YO(g) used in this work for the calculation of the enthalpy of formation of NpO(g) based on the measurements of Ackermann and Rauh [37].

Species	$\Delta_f H_m^o(298.15\ \mathrm{K})/(\mathrm{kJ \cdot mol^{-1}})$	$S_m^o(298.15\ \mathrm{K})/(\mathrm{J \cdot K^{-1} \cdot mol^{-1}})$	Ref.
LaO(g)	−114.2 ± 8.4	239.7 ± 0.3	[55]
YO(g)	−40.12 ± 9.9	233.9 ± 0.3	[55]
La(g)	425.85 ± 4.18	182.272	[55,65]
Y(g)	421.329 ± 3	179.364	[65]

Table B.2
Summary of the heat capacity functions for La(g), LaO(g), Y(g), and YO(g) used in this work for the calculation of the enthalpy of formation of NpO(g) based on the measurements of Ackermann and Rauh [37].

Species	$C_{p,m}^o/(\mathrm{J \cdot K \cdot mol^{-1}}) = A + B \cdot (T/\mathrm{K}) + C \cdot (T/\mathrm{K})^2 + D \cdot (T/\mathrm{K})^3 + E \cdot (T/\mathrm{K})^{-2}$					T/K	Ref.
	A	B	C	D	E		
LaO(g)	27.6756	0.0237	$-2.19208 \cdot 10^{-5}$	$7.38312 \cdot 10^{-9}$	$-1.065474 \cdot 10^{5}$	298–1200	[55]
	49.6554	−0.02233	$1.29576 \cdot 10^{-5}$	$-1.88993 \cdot 10^{-9}$	$-1.476640 \cdot 10^{6}$	1200–3000	
YO(g)	27.5063	0.02279	$-1.95343 \cdot 10^{-5}$	$5.95199 \cdot 10^{-9}$	$-1.036576 \cdot 10^{5}$	298–1200	[55]
	35.5529	0.00285	$1.47240 \cdot 10^{-6}$	$0.289600 \cdot 10^{-9}$	$-6.015959 \cdot 10^{5}$	1200–3000	
La(g)	25.1040	0.00486			$-3.380672 \cdot 10^{5}$	298–2000	[65]
Y(g)	23.0538	−0.000745			$2.694496 \cdot 10^{5}$	298–2500	[65]

Table B.3
Re-assessment of the enthalpy of formation of NpO(g) based on the data of Ackermann and Rauh [37].

Reaction	T/K	$\Delta_f H_m^o(T_{ave})/(\mathrm{kJ \cdot mol^{-1}})$	$\Delta_f H_m^o(\mathrm{NpO,g,298.15\ K})/(\mathrm{kJ \cdot mol^{-1}})$	
			Second law	Third law
NpO(g) + La(g) = Np(g) + LaO(g)	1665–1972	−85.4 ± 4	−2.0 ± 11.4	−6.3 ± 10.6
Np(g) + YO(g) = NpO(g) + Y(g)	1173–1972	−16.8 ± 4	−16.5 ± 12.2	−13.3 ± 11.5

and $\Delta_f H^o_m(\mathrm{NpO,g,298.15\,K}) = -(9.8 \pm 7.8)\ \mathrm{kJ \cdot mol^{-1}}$ for the second and third law analyses, respectively. The latter values are within the uncertainty range of the enthalpy of formation of NpO(g) as selected in the review by Konings et al. [14], i.e., $\Delta_f H^o_m(\mathrm{NpO,g,298.15\,K}) = -(16.6 \pm 10.0)\ \mathrm{kJ \cdot mol^{-1}}$. In this work, the mean value of the third law analysis has been retained, i.e., $\boldsymbol{\Delta_f H^o_m(NpO,g,298.15\,K) = -(9.8 \pm 7.8)\ kJ \cdot mol^{-1}}$ (Table 11), for the reasons detailed above.

Appendix C. Fitting the miscibility gap in the Np–O system

The existence of a miscibility gap in the Np–O system is highly probable by analogy with the U-O and Pu-O systems [2]. Yet, the temperature of the monotectic reaction as optimized herein, i.e., 1117 K, is much lower than suggested by [12]. A higher temperature was found incompatible with the limit of the NpO_{2-x} domain [12] and oxygen potential data over NpO_{2-x} [24]. To illustrate this inconsistency, we present hereafter two alternative models M1 and M2.

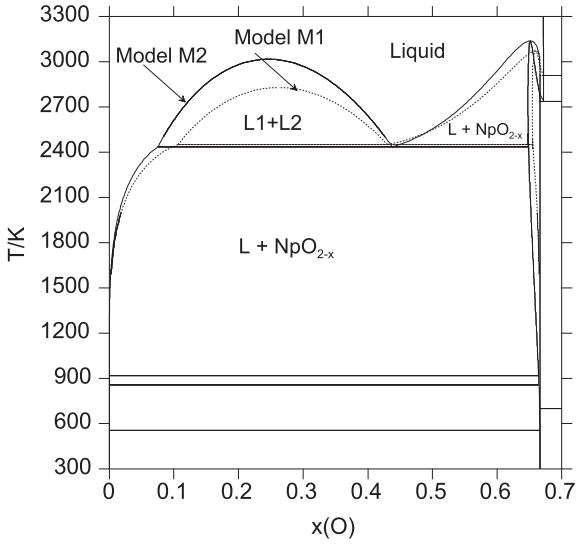

Fig. C.1. Calculated phase diagram for Np–O at 1 bar using the optimized models M1 and M2.

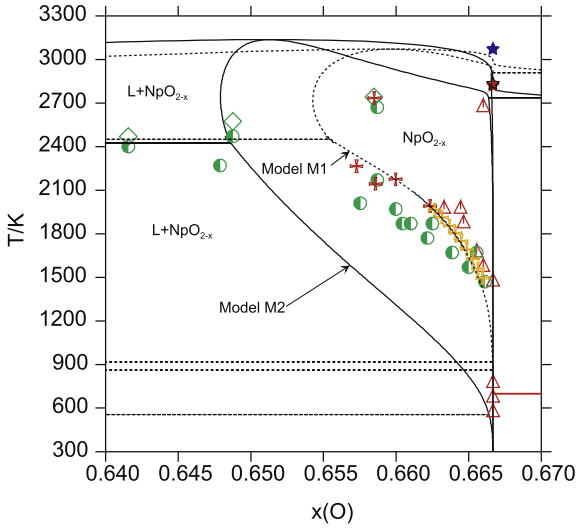

Fig. C.2. Calculated phase diagram for Np–O at 1 bar using the optimized models M1 and M2, and comparison with the experimental data.

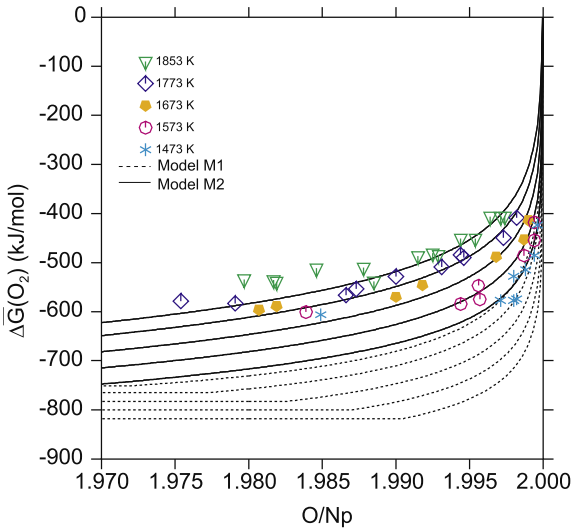

Fig. C.3. Calculated oxygen potential in NpO_{2-x} using the optimized models M1 and M2, and comparison with the experimental data.

In the optimized model M1, the limit of the NpO_{2-x} domain as reported in the literature [12,24] is well reproduced as shown in Figs. C.1 and C.2. The calculated oxygen potential data are found much lower than measured by [24], however (Fig. C.3). The calculated data are even lower than the corresponding curve for the U–O system, which is unreasonable. The liquid phase in equilibrium with NpO_{2-x} is too poor in oxygen in such a configuration. The calculated total pressure at congruent vapourization is in good agreement with the experiment, but the corresponding vapour composition is in strong disagreement with our experimental results. It is calculated as 96.6% NpO_2(g) + 1.8%NpO(g) + 1.6%O(g), which corresponds to an oxygen-to-neptunium ratio $(O/Np)_{azeotrope} = 1.997(3)$ at 2260 K.

In the optimized model M2 the calculated oxygen potential data are in good agreement with [24] (Fig. C.3), but the NpO_{2-x} domain is much wider than reported by [12], with the hypostoichiometric homogeneity range starting around 400 K already (Fig. C.2). The latter phase boundary, like the one calculated by Kinoshita et al, is highly improbable. With this model, the calculated total pressure at congruent vapourization is in good agreement with the experiment, but the corresponding vapour composition is again in strong disagreement with our experimental results. It is calculated as 96.3% NpO_2(g)+2.6%NpO(g)+1.1%O(g), which corresponds to an oxygen-to-neptunium ratio $(O/Np)_{azeotrope} = 1.985(3)$ at 2260 K.

In view of the aforementioned discussion, the three data-sets appear to be conflicting. Experimental investigations of the miscibility gap are therefore highly desirable to confirm its existence, extent and temperature of the monotectic reaction.

Appendix D. Supplementary data

Supplementary data associated with this article can be found, in the online version, at http://dx.doi.org/10.1016/j.jct.2016.07.040.

References

[1] G.L. Hofman, J.H. Bottcher, J.A. Buzzell, G.M. Schwartzenberger, J. Nucl. Mater. 139 (1986) 151–155.
[2] C. Guéneau, N. Dupin, B. Sundman, C. Martial, J.-C. Dumas, S. Gossé, S. Chatain, F. De Bruycker, D. Manara, R.J.M. Konings, J. Nucl. Mater. 419 (1–3) (2011) 145–167.
[3] P. Gotcu-Freis, J.-Y. Colle, C. Guéneau, N. Dupin, B. Sundman, R.J.M. Konings, J. Nucl. Mater. 414 (3) (2011) 408–421.

[4] A. Berche, N. Dupin, C. Guéneau, C. Rado, B. Sundman, J.C. Dumas, J. Nucl. Mater. 411 (1-3) (2011) 131–143.
[5] C. Guéneau, M. Baichi, D. Labroche, C. Chatillon, B. Sundman, J. Nucl. Mater. 304 (2002) 161–175.
[6] C. Guéneau, C. Chatillon, B. Sundman, J. Nucl. Mater. 378 (3) (2008) 257–272.
[7] C. Guéneau, A. Chartier, L. Van Brutzel, Comprehensive Nuclear Materials, 2012, pp. 22–59 (Chapter 2.02).
[8] C.T. Walker, G. Nicolaou, J. Nucl. Mater. 218 (1995) 129–138.
[9] C. Prunier, F. Broussard, L. Koch, M. Coquerelle, in: Proc. Int. Conf. on Future Nuclear Systems: Emerging Fuel Cycles and Waste Disposal Options, page 158, Seattle, USA, 1993.
[10] R.J. Ackermann, R.L. Faircloth, E.G. Rauh, R.J. Thorn, J. Inorg. Nucl. Chem. 28 (1966) 111–118.
[11] P. Gotcu-Freis, J.-Y. Colle, J.-P. Hiernaut, R.J.M. Konings, J. Chem. Thermodyn. 43 (2011) 492–498.
[12] K. Richter, C. Sari, J. Nucl. Mater. 148 (1987) 266–271.
[13] R.J.M. Konings, O. Beneš, J. Phys. Chem. Ref. Data 39 (2010) 043102.
[14] R.J.M. Konings, O. Beneš, A. Kovacs, D. Manara, D. Sedmidubský, L. Gorokhov, V. S. Iorish, V. Yungman, E. Shenyavskaya, E. Osina, J. Phys. Chem. Ref. Data 43 (1) (2014).
[15] J.R. Naegele, L.E. Cox, J.W. Ward, Inorg. Chim. Acta 139 (1987) 327–329.
[16] A. Seibert, T. Gouder, F. Huber, J. Nucl. Mater. 389 (2009) 470–478.
[17] R.J. Lemire, J. Fuger, H. Nitsche, P. Potter, M.H. Rand, J. Rydberg, K. Spahiu, J.C. Sullivan, W.J. Ullman, P. Vitorge, H. Wanner, Chemical Thermodynamics of Neptunium and Plutonium, OECD Nuclear Energy Agency, Data Bank, Issy-les-Moulineaux (France), 2001.
[18] M. Chollet, J. Lechelle, R.C. Belin, J.-C. Richaud, J. Appl. Cryst. 47 (2014) 1008–1015.
[19] O. Beneš, P. Gotcu-Freis, F. Schwörer, R.J.M. Konings, T. Fanghänel, J. Chem. Thermodyn. 43 (2011) 651–655.
[20] R.J.M. Konings, O. Beneš, J. Phys. Chem. Solids 74 (2013) 653–655.
[21] T.D. Chikalla, C.E. McNeilly, J.L. Bates, J.J. Rasmussen, In: High-temperature phase transformations in some lanthanide and actinide oxides, Technical report BNWL-SA-3818, page 351, Odeillo, France, 1971.
[22] R. Böhler, M.J. Welland, F. De Bruycker, K. Boboridis, A. Janssen, R. Eloirdi, R.J. M. Konings, D. Manara, J. Appl. Phys. 111 (2012) 113501.
[23] H. Kinoshita, D. Setoyama, Y. Saito, M. Hirota, K. Kurosaki, M. Uno, S. Yamanaka, J. Chem. Thermodyn. 35 (5) (2003) 719–731.
[24] W. Bartscher, C. Sari, J. Nucl. Mater. 140 (1986) 91–93.
[25] J.A. Lee, K. Mendelssohn, P.W. Sutcliffe, Proc. R. Soc. London, Ser. A 317 (1970) 303.
[26] E.M. Foltyn, J. Nucl. Mater. 172 (1990) 180.
[27] E.J. Huber Jr., C. Holley Jr., J. Chem. Eng. Data 13 (1968) 545.
[28] E.F. Westrum Jr., J.B. Hatcher, D.W. Osborne, J. Chem. Phys. 21 (1953) 419.
[29] L. Merli, J. Fuger, Radiochim. Acta 66/67 (1994) 109–113.
[30] Y.I. Belyaev, V.N. Dobretsov, V.A. Ustinov, Sov. Radiochem. 21 (1979) 386.
[31] H.A. Eick, R.N.R. Mulford, J. Chem. Phys. 41 (1964) 1475–1478.
[32] R.J. Ackermann, E.G. Rauh, J. Chem. Thermodyn. 7 (1975) 211–218.
[33] M. Fred, F.S. Tomkins, J.E. Blaise, P. Camus, Vergés, Atomic spectrum of neptunium, Argonne National Laboratory Technical Report No. ANL 76-68, 1976.
[34] M. Fred, F.S. Tomkins, J.E. Blaise, P. Camus, Verg'es, J. Opt. Soc. Am. 67 (1977) 7.
[35] J. Blaise, P. Luc, J. Vergés, in: Proceedings of the Ninth Conference of the European Group Atomic Spectroscopy, page 20, Cracow, Poland, 1977.
[36] J. Blaise, J.-F. Wyart, J.G. Conway, E.F. Worden, Phys. Scr. 22 (1980) 224.
[37] R.J. Ackermann, E.G. Rauh, J. Chem. Phys. 62 (1) (1975) 108–112.
[38] I. Infante, A. Kovacs, G. La Macchia, A.R.M. Shabi, J.K. Gibson, L. Gagliardi, J. Phys. Chem. A 114 (19) (2010) 6007–6015.
[39] A. Kovacs, R.J.M. Konings, J. Phys. Chem. A 115 (24) (2011) 6646–6656.
[40] J. Rodriguez-Carvajal, Physica B 192 (1993) 55–69.
[41] M. Miller, K. Armatys, Open Thermodyn. J. (7) (2013) 2–9.
[42] J. Drowart, C. Chatillon, J. Hastie, D. Bonnell, Pure Appl. Chem. 77 (4) (2005) 683–737.
[43] A.L. Smith, J.-Y. Colle, O. Benes, A. Kovacs, P.E. Raison, R.J.M. Konings, J. Chem. Thermodyn. 60 (2013) 132–141.
[44] R. Hultgren, R.L. Orr, P.D. Anderson, K.K. Kelley, Selected Values of Thermodynamic Properties of Metals and Alloys, John Wiley & Sons, Inc., 1963.
[45] A.L. Smith, J.-Y. Colle, P.E. Raison, O. Beneš, R.J.M. Konings, J.Chem. Thermodyn. 90 (2015) 199–208.
[46] R.T. Grimley, The Characterisation of High Temperature Vapors, John Wiley & Sons, Inc., New York, 1967.
[47] J.B. Mann, in: T. Hayakawa, K. Ogata (Eds.), Proceedings of the Conference on Mass Spectroscopy, Tokyo, University Park Press, Baltimore, MD, 1970.
[48] D.W Bonnell, J.W. Hastie, Program SIGMA, A Fortran code for computing atomic ionisation cross-sections, NIST, Gaithersburg, MD, unpublished work.
[49] H. Deutsch, K. Becker, T.D. Märk, Int. J. Mass. Spectrom. 167/168 (1997) 503–517.
[50] J.W. Otvos, D.P. Stevenson, J. Am. Chem. Soc. 78 (1956) 546–551.
[51] H. Deutsch, K. Hilpert, K. Becker, M. Probst, T.D. Märk, J. Appl. Phys. 89 (2001) 1915.
[52] O. Beneš, R.J.M. Konings, J.-Y. Colle, J. Nucl. Mater. 462 (2015) 182–190.
[53] L. Dumas, C. Chatillon, E. Quesnel, J. Cryst. Growth 222 (2001) 215–234.
[54] F. Capone, J.-Y. Colle, J.P. Hiernaut, C. Ronchi, J. Phys. Chem. A 103 (1999) 10899–10906.
[55] M. Heyrman, C. Chatillon, A. Pisch, Calphad 28 (2004) 49–63.
[56] P. Clausing, J. Vac. Sci. Technol. 8 (1971) 636–646.
[57] B. Jansson, Tech. Rep. (1984).
[58] B. Sundman, B. Jansson, J.O. Andersson, Calphad 9 (1985) 153–190.
[59] A. Dinsdale, Calphad 15 (1991) 317–425.
[60] M. Hillert, B. Jansson, B. Sundman, J. Agren, Metall. Trans. A 16 (1) (1985) 261–266.
[61] I. Ansara, B. Sundman, Scientific Group Thermodata Europe, Computer Handling and Determination of Data, 1986. North Holland, Amsterdam.
[62] F. Defoort, C. Chatillon, La thermodynamique des gaz U, UO, UO_2 et UO_3 par spectrométrie de masse et techniques d'effusion, Rapport CEA-R-6027, CEA, Saclay 91191, Gif-sur-Yvette, 2003.
[63] C. Younès, Contribution à l'étude thermodynamique par spectrométrie de masse à haute température des oxydes MO_{2-x} [M=U, (U,La), (La,Ce), (La,Ce,Y), (U,Ce)] (Ph.D. thesis), Université de Paris-Sud, Centre d'Orsay, 1986.
[64] Thermo-Calc Console Mode User's Guide Version 3.0. Thermo-Calc Software AB, Foundation of Computational Thermodynamics, Stockholm, Sweden, 2013.
[65] L.B. Pankratz, Bull. 672, U.S. Bureau of Mines, 1982.

JCT 16-340